1978

The Effect of a Horizontal Plane Boundary on a Falling Horizontal Cylinder at Low Reynolds Number.

Yang-jen Chen
Louisiana State University and Agricultural & Mechanical College

INFORMATION TO USERS

This material was produced from a microfilm copy of the original document. While the most advanced technological means to photograph and reproduce this document have been used, the quality is heavily dependent upon the quality of the original submitted.

The following explanation of techniques is provided to help you understand markings or patterns which may appear on this reproduction.

1. The sign or "target" for pages apparently lacking from the document photographed is "Missing Page(s)". If it was possible to obtain the missing page(s) or section, they are spliced into the film along with adjacent pages. This may have necessitated cutting thru an image and duplicating adjacent pages to insure you complete continuity.

2. When an image on the film is obliterated with a large round black mark, it is an indication that the photographer suspected that the copy may have moved during exposure and thus cause a blurred image. You will find a good image of the page in the adjacent frame.

3. When a map, drawing or chart, etc., was part of the material being photographed the photographer followed a definite method in "sectioning" the material. It is customary to begin photoing at the upper left hand corner of a large sheet and to continue photoing from left to right in equal sections with a small overlap. If necessary, sectioning is continued again — beginning below the first row and continuing on until complete.

4. The majority of users indicate that the textual content is of greatest value, however, a somewhat higher quality reproduction could be made from "photographs" if essential to the understanding of the dissertation. Silver prints of "photographs" may be ordered at additional charge by writing the Order Department, giving the catalog number, title, author and specific pages you wish reproduced.

5. PLEASE NOTE: Some pages may have indistinct print. Filmed as received.

University Microfilms International
300 North Zeeb Road
Ann Arbor, Michigan 48106 USA
St. John's Road, Tyler's Green
High Wycombe, Bucks, England HP10 8HR

THE EFFECT OF A HORIZONTAL PLANE BOUNDARY ON A FALLING HORIZONTAL CYLINDER AT LOW REYNOLDS NUMBER

A Dissertation

Submitted to the Graduate Faculty of the
Louisiana State University and
Agricultural and Mechanical College
in partial fulfillment of the
requirements for the degree of

Doctor of Philosophy

in

The Department of Physics and Astronomy

by

Yang-Jen Chen
B.S., Chung Yuan Christian College of Science and Engineering, 1969
M.S., Louisiana State University, 1973
May 1978

DEDICATION

To My Parents

Wu-su Chen

and

Lai-pa Chen

and to my Brothers and Sisters

Mon-chi

Fong-nan

Li-su

Fu-Shiong

Jong-nan

ACKNOWLEDGEMENT

The author is indebted to Professor R. G. Hussey for his guidance, support and encouragement during the entire course of his work.

He also wishes to express his appreciation to Dr. B. Huner for numerous advice and help. Many diverting conversation with Mr. H. Bennett, D. Hensely, J. Stalnaker have made his graduate study a more enjoyable experience.

The author wishes to thank Joanna for her encouragement, understanding and her assistance during the last four years.

A financial assistance pertinent to the publication of this dissertation from Dr. Charles E. Coates Memorial Fund of L.S.U. Foundation donated by George H. Coates is gratefully acknowledged.

Finally, the author would like to thank his parents for their sacrifices, understanding, and for their continued faith in him through his entire graduate study.

TABLE OF CONTENTS

Page

LIST OF TABLES

LIST OF FIGURES

Figure Page

ABSTRACT

Experimental results are presented for the change in velocity of a slender cylinder with its axis horizontal as it falls through a viscous fluid toward a horizontal plane boundary. The Reynolds number based on the diameter of the cylinder ranges from 0.015 to 2.9 . When the relative change in velocity is small (< 15%), it is observed to depend inversely on the square of the distance from the boundary. When the boundary influence is large, the deceleration of the cylinder is observed to be constant, and the velocity extrapolates to zero at the boundary. Calculations based on the theory of de Mestre and Russel do not agree well with the experimental results. Inertia is found to be important, and an attempt is made to calculate the added mass of the decelerating cylinder.

CHAPTER I

INTRODUCTION

In the past few years there has been an increased interest in the study of the motion of bodies in fluids at low Reynolds number. This interest is due primarily to biophysical applications. The Stokeslet singularity was introduced by G.J. Hancock[1] in 1952 to analyze the motion of microscopic organisms through viscous fluids, and since that time a number of specialized mathematical techniques have been developed, including the representation of bodies by distributions of Stokeslets and other singularities, and the use of slender-body theory to simplify the calculations. Theoretical results have been summarized in recent reviews by Lighthill[2] and by Brennan and Winet[3].

Considerable progress has been made in understanding the effects of plane boundaries on the motion of bodies at low Reynolds number. Blake[4], and Blake and Chwang[5] have discussed the image of a Stokeslet in a plane wall. De Mestre[6] used image methods and an extension of Faxen's technique[7] to study several cases of the motion of slender rods near plane boundaries, and de Mestre and Russel[8] have considered additional cases, including some in which the rod rotates. Katz, Blake, and Paveri-Fontana[9] have obtained normal and tangential resistance coefficients for of a slender rod moving near plane boundaries for the case of boundary distance small compared

to rod length. Experimental result have been reported by White[10] and by de Mestre[6] for a horizontal rod falling with its axis parallel to and mid-way between vertical walls. De Mestre[6] has also obtained experimental results for a horizontal rod falling near one vertical wall, and for a vertical rod falling between two vertical walls.

The theoretical results involve a number of simplifying assumptions, the implications of which are not well understood. For example, the use of singularities implies that the Reynolds number is low enough for the Stokes equation to be valid, which implies further that fluid inertia is completely negligible. Except for the simplest shapes (e.g. a sphere), it is not well known how low the Reynolds number must be for this assumption to hold. The lower the Reynolds number, the more important wall effects become; it is not clear where the transition between wall-independent and wall-dominated flow takes place. Finally, when slender body theory is invoked for motion transverse to the long axis of the body, the more slender the body is, the more likely the flow is to be primarily two-dimensional, and then the difficulties associated with the Stokes paradox arise, i.e., inertia may be important even at the lowest Reynolds number.

Although there has been considerable theoretical activity in this field, the only experimental results are those of White[10] and de Mestre[6] which are limited in range. In the work presented here, we report experimental results for a horizontal rod falling at low Reynolds number toward a horizontal plane boundary. The flow

for this case is necessarily unsteady flow since deceleration is involved, so it is necessary to consider the effects of added mass. Although many inviscid flow calculations have been made of added mass in the presence of boundaries, no such solutions are available for viscous flow. Williams and Hussey[15] have considered the infinite fluid viscous flow solution of Stokes for an oscillating cylinder in the limit of quasi-steady flow, and we attempt to apply this solution to the case of monotonically decreasing velocity.

In Chapter II, the basic background of the fundamental singularities and slender-body theory is discussed. Chapter III is concerned with a description of the experimental techniques, the method of data analysis, experimental results and comparison with the theory. Our conclusions are presented and discussed in the same Chapter.

CHAPTER II

BACKGROUND

A. Reynolds Number and Viscous Length

The Reynolds Number R_d is defined as

$$R_d = Ud/\nu$$

where U is a characteristic velocity, d is a characteristic length, and ν is the kinematic viscosity of the fluid. When one considers the motion of a body through a fluid, it is convenient to think of the Reynolds number as the ratio of the body length to a viscous length $\delta = \nu/U$. The viscous length gives an estimate of the range of the viscous force. At the low values of R_d often encounted in biological flows (values of 10^{-3} to 10^{-6} are not uncommon), the viscous length is many times larger than the characteristic body length and often larger than or comparable to the distance from the body to a boundary, so these flows are often strongly influenced by boundary effects. It is not surprising, therefore, that there has been a considerable effort in recent years to calculate the effects of near-by boundaries on the motion of bodies at low Reynolds number.

B. Stokes Equations and Fundamental Singularities

The analysis of the low Reynolds number flow past a slender body has been greatly aided by the development of methods

construct the flow field by means of distributions of fundamental singularities. For the purpose of describing these methods we must explain briefly the nature of the fundamental solutions to the equations of motion.

The forces acting on any element of an incompressible inertialess Newtonian fluid, per unit volume, are a pressure gradient force $-\nabla p$ and a viscous force $\mu\nabla^2\bar{U}$, where p is the pressure, μ is the shear viscosity and $\bar{U}$ is the fluid velocity. The condition that these forces are in equilibrium is

$$-\nabla p + \mu\nabla^2\bar{U} = 0 \tag{1}$$

and the equation of continuity for an incompressible fluid is

$$\nabla\cdot\bar{U} = 0 \tag{2}$$

Equations (1) and (2) are called the Stokes equations. If an external force term $\bar{f}$ per unit volume is introduced in (2), i.e.

$$\nabla p = \mu\nabla^2\bar{U} + \bar{f} \tag{3}$$

then Equation (3), along with Equation (2), is called the inhomogeneous Stokes Equation. The solutions of (3) corresponding to forces having singular behaviour in an unbounded fluid flow have been called by Chwang and Wu[24] the fundamental solutions, and the forces are called the fundamental singularities.

The primary fundamental solution is called a Stokeslet and is associated with a singular point force located at the origin

$$\bar{f}_s = 8\pi U\bar{\alpha}\delta(\bar{r}) \tag{4}$$

where $\bar{\alpha}$ is a constant vector, $\delta(\bar{r})$ is the Dirac delta function, and $\bar{r}$ is the position vector. The resulting fluid velocity and pressure are respectively

$$\bar{U}_s(\bar{r};\bar{\alpha}) = \bar{\alpha}/r + (\bar{\alpha}\cdot\bar{r})\ \bar{r}/r^3 \tag{5}$$

$$p_s(\bar{r};\bar{\alpha}) = 2\mu\bar{\alpha}\cdot\bar{r}/r^3 \tag{6}$$

where $r = |\bar{r}|$ and $\bar{\alpha}$ denotes the Stokeslet strength and direction. The velocity field of a Stokeslet falls off like r^{-1} at large distance, and the pressure p decreases like r^{-2} . A derivative of any order of this solution is also a solution to the basic equation. Thus, higher order singularities can be constructed, such as a Stokes doublet, Stokes quadrupole, etc. Batchelor[14] has shown how to decompose a Stokes doublet into an antisymmetric component (called a couplet or rotlet) representing the flow field due to a singular point torque and a symmetric component (called a stresslet) representing a pure straining of the fluid. The Laplacian of the Stokeslet solution leads to a potential doublet of strength $\bar{\delta}$ for which

$$U_D = -\bar{\delta}/r^3 + 3(\bar{\delta}\cdot\bar{r})\bar{r}/r^5 \ ;\ p_D = 0 \tag{7}$$

since p_s is a harmonic function of $\bar{r}$ which has zero vorticity. The potential doublet has the same form as in inviscid, potential flow, but its contribution to the pressure is now zero, so it has no inertial effect.

Hancock[1] used a linear superposition of these singularities to simulate the fluid mechanics of flagellated microorganisms. Chwang[27] and Wu and Chwang[24] have used distributions of these singularities to obtain Stokes flow solutions for prolate spheroids, spheres, and cylinders in a wide range of flow fields, such as shear flows, flows with a parabolic profile, and extensional flows. Furthermore, they have introduced new singularities that enable them

to treat "interior" Stokes flows, i.e. flows in which the fluid is completely enclosed in a container of simple shape. All of these solutions are exact only at zero Reynolds number. The contribution of inertia at low but non-zero Reynolds number may require re-examination of the far-field, where the inertia terms may become important, particularly if the geometry is primarily two dimensional.

C. The Treatment of Boundaries

As noted earlier, when the Reynolds number is very small, viscous effects are long ranged, so boundaries can have a significant influence on the motion of a body through the fluid. For potential flow of an inviscid fluid, many techniques are available for calculating boundary effects (see, for example, Lamb's[13] treatise and Appendix I of this dissertation); since only the normal component of the velocity is restricted at the boundary, the boundary conditions are relatively easy to meet. For viscous flows, however, both the normal and tangential components are specified at the boundary, so solutions are more difficult. In spite of the difficulty, Blake[4] and Blake and Chwang[5] have succeeded in obtaining images for some of the basic singularities near plane boundaries. Blake's solution for a Stokeslet in the presence of a stationary plane boundary is as follows

$$U_i = \alpha_j \Big(\Big(\frac{\delta_{ij}}{r} + \frac{r_i r_j}{r^3} \Big) - \Big(\frac{\delta_{ij}}{R} + \frac{R_i R_j}{R^3} \Big) + 2h(\delta_{j\beta}\delta_{\beta k} - \delta_{j3}\delta_{3k}) \times$$

$$\frac{\partial}{\partial R_k} \Big\{ \frac{hR_i}{R^3} - \Big(\frac{\delta_{i3}}{R} + \frac{R_i R_3}{R^3} \Big) \Big\} \Big) \qquad (8)$$

$$p = \alpha_j \left(\frac{r_j}{r^3} - \frac{R_j}{R^3} - 2h(\delta_{j\beta}\delta_{\beta k} - \delta_{j3}\delta_{3k}) \frac{\partial}{\partial R_k} \left(\frac{R_3}{R^3} \right) \right) \tag{9}$$

$$r = \left[(x_1 - y_1)^2 + (x_2 - y_2)^2 + (x_3 - h)^2 \right]^{\frac{1}{2}}$$

$$R = \left[(x_1 - y_1)^2 + (x_2 - y_2)^2 + (x_3 + h)^2 \right]^{\frac{1}{2}}$$

where $\beta = 1, 2$. The Stokeslet is situated at (y_1, y_2, h) and the image is at $(y_1, y_2, -h)$. The image system is found to consist of a Stokeslet equal in magnitude but opposite in sign to the initial Stokeslet, a Stokes-doublet and a source-doublet.

Blake and Chwang derived similar image systems for a couplet, a source, and a potential doublet. An important effect of the presence of the wall is that the nature of the far-field is altered. A Stokeslet oriented parallel to a wall leads to a far field which is a Stokes doublet, decaying like r^{-2} rather than the r^{-1} of a Stokeslet in an unbounded fluid. The far field of a Stokeslet oriented perpendicular to a wall is like a Stokes quadrupole or a potential doublet, which decays like r^{-3}.

D. Slender-Body Theory

A rigid body is considered to be a slender body if its length 2ℓ is large compared with its diameter d, and the thickness to length parameter defined by $\varepsilon = \{ \ell n(4\ell/d) \}^{-1}$ is small. The basic idea in slender-body theory for Stokes flow is that the disturbance due to the presence of the body is approximately the same as that due to a line distribution of fundamental singularities. The slender-body theory for Stokes flow was initiated by

Burgers[28]. The elementary form of the theory suggested was improved by Broersma[29, 30], and the theory in more general form has been developed considerably[14, 31, 32, 33] in recent years. Most of these published works are concerned with slender bodies of circular cross-section. Recently, Batchelor[14] has investigated such flows for bodies of arbitrary cross-section.

From the previous discussion of fundamental singularities we understand that the velocities induced at the point on the surface by singularities outside a certain near-field will be dominated by Stokeslets in the far-field, since Stokeslets have a far field effect like r^{-1} which dominates that of the other singularities. Thus, the primary distribution along the line of the entire axis of the slender body is one of Stokeslets. The boundary condition at the cross-section under consideration is satisfied by introducing a potential doublet or other necessary singularities.

The most important step for the application of slender-body theory is to find the strength and direction of the Stokeslets distributed along the entire axis of the slender body plus the local distribution of higher order singularities that satisfy the required boundary condition. The result of the induced velocity for a slender body will be complicated integral equations, and these can be simplified to obtain approximate solutions for the flow around such slender body by taking advantage of the slenderness.

E. Wall Effect on Slender-Body Motion

The motion of a body at low Reynolds number is

clearly altered by the presence of a nearby boundary. There have been a significant number of recent papers on the influence of nearby boundaries for slender cylindrical rods. An earlier paper by Brenner[34] gave results for more general shapes when the wall effects are small.

Consider the problem of a cylindrical rod of diameter d and length 2ℓ moving through a viscous fluid with its axis a distance h away from the wall. De Mestre[6] has studied such a slender rod falling in a horizontal orientation i) parallel to a fixed vertical plane and ii) midway between two vertical parallel plane walls, and iii) in a vertical orientation midway between two vertical parallel plane walls. De Mestre and Russel[8] have presented analytical results for two cases in which the rod rotates, namely axial fall parallel to a plane vertical wall, and transverse fall in a vertical plane normal to a vertical wall. The related cases of axial and transverse fall toward a horizontal wall are also treated. In these cases, de Mestre and de Mestre and Russel have examined the wall effect for general values of ℓ/h (both large and small).

For the case of a cylinder parallel to the wall and approaching it with velocity U as shown in Fig.1A, de Mestre and Russel solved the problem by not only employing distributions of Stokeslets in the x_1 and x_3 direction but also including an axial distribution of source-doublets in the x_3 direction with the appropriate image system to satisfy the no-slip condition at the wall. The resulting integral equations were solved by an asymptotic expansion suggested by Batchelor[14] for small values of both d/2h

and $d/2\ell$. The total drag on the cylinder was found to be*

$$F' = -4\pi\mu U\varepsilon\ell \{ 2+\varepsilon(-0.386+W) + O(\varepsilon^2, \varepsilon d/h)\} \quad (10)$$

with W representing the wall effect. When W is O(1) or greater, the wall effect is given by

$$W = 2 \operatorname{arcsinh}(\ell/h) + \{ 1+(h/\ell)^2\}^{-\frac{1}{2}} \quad (11)$$

As $\ell/h \to 0$, Eq.(10) becomes

$$F' = -4\pi\mu U\varepsilon\ell \{ 2+\varepsilon(-0.386+3\ell/h) + O(\ell^3/h^3, \varepsilon^2)\} \quad (12)$$

while as $h/\ell \to 0$ ($\ell >> h >> d$)

$$F' = -8\pi\mu U\ell \{ \ln(4h/d)-1\}^{-1} \quad (13)$$

Equations (12) and (13) agree respectively with the results given by Brenner[34] and Lighthill[2] .

Katz, Blake and Paveri-Fontana[9] have made a similar calculation but with the assumption that the boundary distance is small compared to the rod length, i.e., $R \ll h \ll \ell$. They examined this situation by constructing the flow from a distribution of Strokeslets along the axis of the rod and satisfying the no-slip condition at the wall by adding the appropriate image system, but they omitted additional singularities because they are of higher order. The resulting equation were solved by a technique developed by Tillett[34] and Cox[32] . The solution obtained agrees with Eq.(13).

* typographical error has been corrected.

CHAPTER III

I. EQUIPMENT AND PROCEDURES

A. Experiment

Experiments were carried out with the arrangement illustrated in Fig. 1. A small cylindrical rod with its axis horizontal was allowed to fall in a viscous liquid contained in a glass-walled tank. By means of a stroboscope, multiple images of the cylinder were produced on a single frame of photographic film. The distance and the time interval between images were used to obtain values of the velocity of the falling cylinder as it approached the bottom of the tank.

The tank has a rectangular base 50 x 26 cm and it was filled to a depth of 23 cm with a silicone liquid. Silicone liquids were used to provide a wide viscosity range with a small temperature coefficient of viscosity. Three values of kinematic viscosity were used, nominally 0.5, 1, and 4 cm^2/sec. For each liquid, the kinematic viscosity ν and density ρ were determined as functions of temperature; viscosities were measured with Cannon-Fenske routine viscometers and densities were measured with an analytical balance. During the experiment the viscosity and density were obtained indirectly from the fluid temperature, which was monitored by a thermistor with an analog readout (Yellow Springs Model 46, used with a Hewlett-Packard 7101B strip-chart recorder). The thermistor

was calibrated with an accurate mercury-in-glass thermometer. The temperature variation of the fluid was within $0.7^{o}C$ for a series of drops (about 30 drops in 4 hours).

The rods were made from steel drill blanks; two sizes were used, no.61 and no.75 (American Standard Twist Drill numbers). The end surfaces were ground flat and perpendicular to the cylinders axis. Values of the length 2ℓ, diameter d, and mass m of cylinders are given in Table I, along with the length to diameter ratio, and the parameter $\varepsilon = \{ \ln(4\ell/d) \}^{-1}$.

An Asahi Pentax SP 35mm camera with focal length 50mm was used with Kodak 2475 film (ASA 1000). The light source was a General Radio 1531A Strobotac which was triggered by pulses from a Hewlett Packard 5326B counter-timer. A frequency divider was used to provide a choice of 20, 10 or 5 pulses per second for the light source.

To fix the length scale in the photographs, pictures were taken of a flat glass scale held vertically in the plane of fall of the cylinders. The scale had markings at 1 mm intervals. Before the rods were dropped, 3 to 5 pictures of the length scale in the fluid were taken successively in each roll of film.

An electromagnetic dropper was used to hold and release the cylinders in the fluid. Before being dropped, the cylinders were demagnetized by passing them through a degaussing coil. Cylinders of the same diameter were dropped in the order of decreasing length. Sometimes, because of a faulty release, the cylinder did not fall with its axis horizontal. Therefore, each cylinder was photographed 4 to 10 times, and the picture of the best drop was selected for measurement.

The largest source of error in this experiment was in setting the measuring line of the travelling microscope on the bottom line of an image on the film. This setting was reproducible to within 1 μm. The smallest distance measured was 40 μm, so the maximum error was 2.5%. However, this occurred only for images close to the wall. Except for those few cases, the distances had values ranging from 100 to 800 μm, so the hairline setting error was 1% or less for most of the distances. Other direct sources of error were less than 1%. The effects of the sidewalls and the free surface are discussed subsequently.

B. Analysis of the Data

Position measurements were taken directly from the film by means of a travelling microscope which could be read to within 0.5 μm. A magnification factor M was determined by measurements on photographs of the length scale; M is defined as the ratio of the distance measured on the photograph of the length scale to the actual distance on the scale. M was found to depend slightly on position on the film. This dependence could be represented by

$$M(L') = a - b(c - L') \text{ for } c>L'$$
$$\text{and} \quad M(L') = a + b'(c - L') \text{ for } c<L' \qquad (1)$$

where c is the position of maximum magnification and L' is the distance (on the film) from the bottom of the tank. With the camera 32 cm from the sidewall of the tank, typical values were a=0.1501, $b=8.9\times10^{-4}\,cm^{-1}$, $b'=7.5\times10^{-4}\,cm^{-1}$, and c=1.109cm. The maximum variation in M was 0.96%.

Let D_i' represent the distance (on the film) between successive images of the cylinder. These distances were measured from the lower edge of the image. D_1' is the distance from the bottom of the tank to the image closest to the bottom. The time interval for the cylinder to fall this distance is not known. The time interval Δt for the cylinder to fall the other distances D_2', D_3', etc. (taken in order from the bottom up) is known from the firing rate of the stroboscope. The midpoint of the distance intervals is given by $L_1'=\frac{1}{2}D_1'$ and

$$L_i' = \sum_{j=1}^{i-1} D_j' + \tfrac{1}{2}D_i' \qquad i = 2,3,\text{---}. \tag{2}$$

The magnification M_i at the midpoint was calculated from Eq.(1) and the actual distance was obtained from

$$D_i = D_i'/M_i(L_i'). \tag{3}$$

The mean velocity is given by

$$U_i = D_i/\Delta t\ , \tag{4}$$

and the position L_i at which the cylinder has this velocity was taken to be the midpoint of the interval,

$$L_i = \sum_{j=1}^{i-1} D_j + \tfrac{1}{2}D_i \qquad i = 2,3,\text{---}. \tag{5}$$

The use of Eq.(4) is based on the assumption that the time interval is small enough for a linear approximation to be accurate. This assumption was tested by fitting the data with quadratic and cubic equations; the velocities calculated from these equations agreed with those obtained from the linear approximation to within

0.5%. The displacements D_i for cylinder no. 61A moving in fluids of nominal kinematic viscosity 0.5, 1, and 4 cm^2/sec are given in Table II. The constant values of displacement obtained when the cylinder was far from the bottom were averaged, and the average value was used to calculate the constant terminal velocity U_∞ . Values of U_∞ are given in Table III.

II. EXPERIMENTAL RESULTS

After release, the cylinders accelerated from rest to terminal velocity and maintained this velocity until they were within 2 to 8 cm of the bottom. At that point, the velocity began to decrease and within the last few mm the deceleration was constant. The velocity approached zero as the cylinder approached the bottom. Let U be the cylinder velocity and $\Delta U = U_\infty - U$. It is convenient to present the experimental results in three regions: the far field ($\Delta U/U_\infty < 0.005$), the transition region ($0.005 < \Delta U/U_\infty < 0.5$), and the near field ($0.5 < \Delta U/U_\infty$) .

A. The Far Field Region ($\Delta U/U_\infty < 0.005$)

In this region the cylinder falls with a constant terminal velocity U_∞. The effect of the sidewalls was found to be small (see subsequent discussion). The drag F is equal to the effective weight (weight minus buoyant force). F was measured directly by weighing the cylinders in the liquid as described by Huner and Hussey[11]. The dimensionless drag $C = F/8\pi\mu U\ell$ is plotted versus R_d in Fig.2. The closed symbols are the values calculated from the measured velocities U_∞ given in Table III. The open symbols are values calculated from

velocities extrapolated to infinite cylinder length in the manner of Huner[11]. The open symbols agree well with the empirical relation given by Huner:

$$C = \sigma - 0.87\sigma^3 + 0.514\{1 - \exp(-R_d)\}\sigma^4 \qquad (6)$$

where $\sigma = \{\tfrac{1}{2} - \gamma - \ln(R_d/8)\}^{-1}$ and γ is Euler's constant. Also shown in Fig.2 are the theoretical results of Kaplun[12] ($C = \sigma - 0.87\sigma^3$) and Lamb[13] ($C = \sigma$) for cylinders of infinite length. The horizontal lines are the theoretical results of de Mestre and Russel[8] for finite length cylinders in the limit $\ell/h \to 0$, where h is the distance from the cylinder axis to the bottom wall. In this limit, de Mestre and Russel's result is

$$F'_\infty = -4\pi\mu U_\infty \ell\varepsilon(2 - 0.386\varepsilon). \qquad (7)$$

A typographical error (1.386 instead of 0.386), pointed out by Brennan and Winet[3], is corrected here. Eq.(7) is consistent with the more general result of Batchelor[14], which, when specialized to the case of a circular cylinder, gives $C = \varepsilon(1 - 0.193\varepsilon + 0.215\varepsilon^2)$.

By measuring the distance between images separated by several time intervals, it was possible to put more stringent limits on the change in velocity. For example, for cylinders 75A at $R_d = 0.0154$ and 75E at $R_d = 0.0181$, the velocity varied less than 0.4% for $8.5 \leq L \leq 13$ cm.

B. The Transition Region ($0.005 < \Delta U/U_\infty \leq 0.5$)

A correlation of the experimental results for this region is shown in Fig.3. L is the distance from the bottom wall to the nearest edge of the cylinder. Figure 3 is a log-log plot of $\Delta U/U_\infty$

versus L made dimensionless by powers of the cylinder length 2ℓ, the diameter d, the velocity U, and the kinematic viscosity ν. The powers were chosen empirically to give the best correlation. The Reynolds number based on diameter has the range

$$0.0154 < R_d = U_\infty d/\nu < 2.86 \tag{8}$$

and based on length

$$0.37 < R_\ell = 2\ell U_\infty/\nu < 122. \tag{9}$$

For $0.005 < \Delta U/U_\infty < 0.15$, the results in Fig.3 are well represented by a line of slope -2. The straight line in Fig.3 is the equation

$$\Delta U/U_\infty = 0.60(\Lambda/L)^2 \tag{10}$$

where

$$\Lambda = \nu^{0.4} d^{0.325} (2\ell)^{0.275}/U^{0.4} \quad . \tag{11}$$

The effect of the bottom boundary will be less than 1% if $L > 7.75\Lambda$ and less than 0.5% if $L > 10.95\Lambda$.

C. The Near Field Region ($0.5 < \Delta U/U_\infty$)

Fig.4 is a log-log plot of U/U_∞ versus L made dimensionless with powers of ℓ, d, ν, and U_∞ . The best correlation was obtained with slightly different powers than in the transition region and with U_∞ used instead of U. The straight line in Fig.4 is given by

$$U/U_\infty = 0.607 \{ L^{0.6} U^{0.12} \nu^{-0.12} (2\ell)^{-0.18} d^{-0.30} \} \tag{12}$$

When U/U_∞ is plotted versus time, it is found that the deceleration over most of the near field is constant. In five cases the region of constant deceleration was extensive enough for accurate measurements to be made. Information on these five cases is presented

in Tables IV and V. Table IV includes the constant value of the deceleration d^2L/dt^2 and the time interval Δt between stroboscope flashes. Table V contains the observed displacements in the constant deceleration region. Positions (measured from the bottom of the tank to the nearest edge of the cylinder) can be obtained by summing the displacements: $L_j = \sum_{i=1}^{j} D_i$. When the deceleration is known to be constant, it is possible to make a more exact identification between positions and velocities: If L_{i+1} , L_i , and L_{i-1} are the positions at times $t - \Delta t$, t, and $t + \Delta t$ respectively, then the instantaneous velocity at time t and position L_i is $(L_{i+1} - L_{i-1})/2\Delta t$. Velocities calculated in this manner from the data in Table V are shown in Fig.5. The results are consistent with the relation

$$-dL/dt = \{ 2L(d^2L/dt^2) \}^{\frac{1}{2}} \qquad (13)$$

which implies that the velocity approaches zero as the cylinder approaches the bottom wall. Closer examination of individual cases reveals that the extrapolated position of zero velocity is zero within ± 0.2 mm.

When the constant deceleration $-dU/dt$ is made dimensionless by dividing by U_∞^2/d as shown in Fig.6, the resulting values are only weakly dependent on the Reynolds number R_d and the length to diameter ratio $2\ell/d$. The straight line in Fig.6 is a least squares fit to the data; the equation of this line is

$$(-dU/dt)(d/U_\infty^2) = 0.1157(R_d d/2\ell)^{0.19} \ . \qquad (14)$$

There is a slight discrepancy between Eqs. (13) and (14) and Eq.(12). If Eqs. (13) and (14) are combined and solved for U/U_∞ ,

the result is

$$U/U_\infty = 0.481 \{ L^{0.5} U^{0.095} \nu^{-0.095} (2\ell)^{-0.095} d^{0.31} \} \quad . \quad (15)$$

This result is quite similar but not identical to Eq. (12). The reason for the discrepancy is that Eqs. (13) and (14) are restricted to data for which the deceleration is constant, but Eq. (12) is an empirical correlation of a larger collection of data, including some outside of the constant deceleration region.

D. The Effect of Other Boundaries

The cylinder velocity is influenced slightly by the distance H between the nearest sidewalls (those parallel to the cylinder axis). This influence was studied by using different values of H (from 25.7 to 4.85 cm) with cylinder no. 61A falling in the 4 cm^2/sec fluid. The results, shown in Fig.7, agree well with the empirical formula obtained at higher R_d by Huner[11] . If U_H is the velocity measured when the cylinder is far from the bottom and U_∞ is the value of U_H obtained as $H \to \infty$, then Huner's result can be written

$$U_\infty/U_H = 1 + 3.60\nu(2\ell d)^{\frac{1}{2}}(H^2 U_H)^{-1} \quad (16)$$

Our measurements indicate that Huner's formula is still valid at $R_d = 0.10$. If we assume that the same relation holds at the lowest R_d used in this experiment ($R_d = 0.0154$), then for H = 25.7 cm, the sidewall influence on U_H is never greater than 0.5%. Changing H from 25.7 to 4.85 cm at $R_d = 0.10$ had no noticeable influence on $\Delta U/U_\infty$ in the transition region or on U/U_∞ in the near field.

The effect of the endwalls (those perpendicular to the

cylinder axis) was not studied experimentally but was presumed to be negligible since the distance between them (50 cm) was about twice the maximum distance between the sidewalls. The influence of the free surface was found to be approximately symmetrical to the influence of the bottom wall and therefore was less than 0.5% for depths greater than 8 cm.

III. THEORY

A. Added Mass Coefficient

A solid body moving in a fluid shows an apparent increase in mass. This increase, called added mass, is due to the inertia of the fluid but is also influenced by viscosity. The presence of a fixed boundary increases the added mass. The added mass coefficient k is defined as the ratio of the added mass to the mass of fluid displaced. For a circular cylinder of diameter d oscillating in a straight line normal to its axis with circular frequency ω in a fluid of kinematic viscosity ν , the added mass coefficient is given by[15]

$$k_1(\nu,\omega) = 1 - (4N_1/xN_0)\cos(\phi_1 - \phi_0 - \tfrac{3}{4}\pi) \qquad (17)$$

where N_n and ϕ_n are, respectively, the modulus and phase of the Kelvin function $\ker_n x + i\,\mathrm{kei}_n x$ and $x = \tfrac{1}{2}d(\omega/\nu)^{\frac{1}{2}}$. This result, due originally to Stokes, is based on the assumptions $(2\nu/\omega)^{\frac{1}{2}} \ll d$ and $A \ll d$, where A is the amplitude of the oscillation. However, Williams and Hussey[15] have shown that Stokes' theory agrees with experiment for $(2\nu/\omega)^{\frac{1}{2}}$ as large as 2d , with $A \simeq d$, and for the oscillational Reynolds number

$\omega Ad/\nu$ as small as 10^{-3} .

In the absence of a more rigorous solution, we shall assume that Eq. (17) can be used to calculate the added mass coefficient for a cylinder with monotonically decreasing velocity. The "frequency" is calculated as follows: We assume that the small section of the U vs. t curve between t and $t + \Delta t$ can be approximated by a section of the curve $U = U_\infty \cos\omega t$, with $0 < \omega t < \frac{1}{2}\pi$. Let U and $U - \Delta U$ be the velocities at t and $t + \Delta t$, respectively. Then

$U - \Delta U = U_\infty \cos\omega(t + \Delta t) = U(\cos\omega\Delta t - \tan\omega t \sin\omega\Delta t)$ and

$\tan\omega t = \beta = \{ (U_\infty/U)^2 - 1\}^{\frac{1}{2}}$. If

$\omega\Delta t \ll 1$, then $(\omega\Delta t)^2 + (2\tan\omega t)(\omega\Delta t) - (2\Delta U/U) = 0$ and

$$\omega\Delta t = \{ \beta^2 + (2\Delta U/U)\}^{\frac{1}{2}} - \beta \ . \qquad (18)$$

We assume further that the presence of the boundary has a direct effect only on the inviscid part of k_1 . The inviscid boundary effect can be calculated by replacing the cylinder with a potential doublet and using image methods[16] to account for the boundary. The result is that the inviscid added mass coefficient is given by

$$k(\text{inv}) = 1 + 2\alpha^2 + \frac{2\alpha^4}{(1-\alpha^2)^2} + \frac{2\alpha^6}{(1-2\alpha^2)^2} + \frac{2\alpha^8}{\{(1-\alpha^2)^2-\alpha^2\}^2} + \text{---} \qquad (19)$$

where $\alpha = d/4h$ and h is the distance of the cylinder axis from the boundary. If we represent k(inv) by $1 + k(\alpha)$, then the total added mass coefficient is

$$k = k(\alpha) + k_1(\nu,\omega) \ . \qquad (20)$$

B. Calculation of the Change in Velocity

De Mestre and Russel[8] have derived an expression for the force F' on a cylinder of length 2ℓ and diameter d moving with velocity U toward a parallel plane boundary a distance h away from the cylinder axis. When the effect of the boundary is small ($d \ll \ell \ll h$), their expression can be written

$$F' = -4\pi\mu U\varepsilon\ell \{ 2 + \varepsilon(W - 0.386) + O(\varepsilon^2, \varepsilon d/h) \} \qquad (21)$$

where μ is the viscosity, $\varepsilon = \{ \ln(4\ell/d) \}^{-1}$, and

$$W = 2 \operatorname{arcsinh} (\ell/h) + \{ 1 + (h/\ell)^2 \}^{-\frac{1}{2}} . \qquad (22)$$

W is equal to $3\ell/h$ within 3% for $W < 1$. When the boundary effect is large ($d \ll h \ll \ell$) , their expression becomes

$$F' = -8\pi\mu U\ell \{ \ln(4h/d) - 1 \}^{-1} . \qquad (23)$$

Eq. (23) has also been obtained by Lighthill[2] and by Katz, etal[9] .

In Fig.2 we have shown that in the range of Reynolds number of this experiment, the far field experimental drag does not agree with the far field limit of Eq. (21). Therefore, in order to compare the observed change in velocity with that predicted by Eq. (21), it is necessary to normalize the far field drag values. This is done as follows: Let F_∞ be the observed drag when the cylinder is far from the wall. We define the calculated drag as

$$F = F_\infty F'/F'_\infty \qquad (24)$$

where F' and F'_∞ are obtained from Eqs. (21) and (7) respectively.

When the cylinder is far from the bottom, $F = F_\infty$ and the

drag is balanced exactly by the effective weight of the cylinder. When the cylinder enters the influence of the bottom, the drag increases, and the deceleration of the cylinder is given by

$$dU/dt = - (F - F_\infty)/ m^* \tag{25}$$

where $m^* = m + km'$, m is the mass of the cylinder, k is given by Eq. (20), and m' is the mass of the displaced fluid. A finite difference form of Eq. (25) is used to calculate the velocity as follows: A starting position h_0 is chosen and the velocity U_0 at this position is taken to be the experimental value of U_∞ . The next position h_1 is calculated from $h_1 = h_0 - U_0\Delta t$, and the next velocity U_1 is calculated from the finite difference form of Eq. (25) with F calculated from Eq. (24). The value of k is not known at this point, so it is arbitrarily started at $k = 1$. Subsequent values of the velocity, U_2, U_3, etc., are calculated in the same manner but with k now calculated from Eq. (20). The finite difference equations are:

$$h_i = h_{i-1} - U_{i-1}\Delta t \tag{26}$$

$$U_i = U_{i-1} - (F_i - F_\infty)\Delta t/m^* \tag{27}$$

$$\beta_i = \{ (U_\infty/U_{i-1})^2 - 1\}^{\frac{1}{2}} \tag{28}$$

$$\omega_i = (\{ \beta_i^2 + 2(U_{i-1} - U_i)/ U_{i-1}\}^{\frac{1}{2}} - \beta_i)/\Delta t \ . \tag{29}$$

Values of the added mass coefficient k and the frequency ω were found to depend on starting position h_0 in the initial stages of the calculation, as shown in Fig. 8, but to approach rapidly a

curve that was independent of h_0 . The values of k calculated in this manner were quite large, ranging from 27,000 (cylinder 75E, ν=4 cm^2/sec, L/Λ=12.2) to 24 (cylinder 61A, ν=0.5 cm^2/sec, L/Λ=0.045). However, the deceleration $\Delta U/\Delta t$ was small when k was large and vice versa, so the ratio of inertial force $(m + km')\Delta U/\Delta t$ to the drag F_∞ had its smallest value (1.3%) at maximum k and its largest value (29.4%) at minimum k .

C. Comparison with Experiment

The results calculated from the theory of de Mestre and Russel { Eqs. (21) and (22)} are compared with our experimental correlation in Fig.9 . The experimental curve is a smooth curve drawn through the data of Fig.3. The theoretical results were calculated (as described in the previous section) for values of cylinder geometry and fluid viscosity corresponding to the experiment. In addition, a theoretical curve was obtained for the geometry of cylinder 75E and a viscosity of 6 cm^2/sec (R_d = 0.0025). It is apparent that for the range of Reynolds number investigated here, the calculated curves are not correlated by the same parameters as the experimental values. In general, the theoretical curves give larger values of $\Delta U/U_\infty$ than observed for $L/\Lambda > 4$ and smaller values than observed for $L/\Lambda < 0.6$. Moreover, the theoretical and experimental curves are of sufficiently different shape that it is unlikely they would coincide in the limit $R_d \to 0$.

The influence of added mass on the calculated curves is shown in Fig.10 . The curve calculated as described in the previous

section (with variable added mass coefficient k) is compared with curves calculated with constant values of k. The curves for $k = 0$ and $k = 100$ coincide and give values of $\Delta U/U_\infty$ that are consistently higher than the variable k curve. Along the variable k curve, the values of k range from 27,000 to 700 , and the constant k curves for $k = 10{,}000$ and $k = 1{,}000$ cross the variable k curve at points where the values of k are approximately the same. For such large values of k, the inviscid contribution to the added mass {Eq.(19)} is insignificant.

In Fig.11 the experimental results in the near field are compared with results calculated from Eq.(23). The calculated values were obtained in the same manner as in the transition region {i.e., by use of Eqs.(24) and (26) through (29)} but the calculations were started at particular experimental values of position and velocity (usually those for which $\Delta U/U_\infty \simeq 0.1$). However, the calculated results in the near field were quite insensitive to the starting values. As shown in Fig.11 , the calculated values of U/U_∞ are generally smaller than the observed values, and the shapes of the calculated and experimental curves are different. The calculated curve at $R_d = 0.0025$ shows that the experimental curve is not simply a limit approached as $R_d \to 0$.

IV. DISCUSSION

A. The Far Field Region

The experimental values of the dimensionless drag for cylinders of finite length (closed symbols in Fig.2) are consistently

higher than the theoretical values of de Mestre and Russel or of Batchelor. As the Reynolds number is lowered, the experimental values appear to be approaching the theoretical curves from above. Experiments with $R_d < 10^{-2}$ are needed to determine if there is some value of R_d below which the dimensionless drag depends only on the geometrical parameter ε . We stress again the difficulty and importance of properly accounting for the influence of all boundaries in experiments at very low R_d .

When the experimental velocities are extrapolated to infinite cylinder length (by plotting 1/U versus $1/\ell$) as described by Huner, the results agree well with the empirical formula of Huner, and for $R_d < 0.2$ with the theoretical results of Lamb and of Kaplun for cylinders of infinite length. However, as R_d is lowered, the size of the correction (as indicated by the difference between the open and closed symbols in Fig.2) becomes so large that the extrapolation procedure becomes questionable. It appears that when the Reynolds number based on length is less than 1, it is no longer appropriate to regard a long finite cylinder as a section of an infinite cylinder.

The theory of de Mestre and Russel {Eqs.(21) and (22)} predicts a bottom wall effect that is relatively long ranged, varying as ℓ/h . As h changes from 13 cm to 8.5 cm, the relative change in the drag $(F' - F'_\infty)/F'_\infty$ predicted by the theory ranges from 3.4% to 5.1% for cylinder 75A and from 2% to 3% for cylinder 75E. However, the observations indicate that at $R_d \simeq 0.02$, the velocity was constant to within 0.4% for these cylinders over that range of h . This difference between experiment and theory, unlike those shown in Fig.9,

is not dependent upon any assumptions about added mass.

B. The Transition Region

There is a striking similarity between Huner's result for the influence of the sidewalls {Eq.(16)} and our result for the influence of the bottom for $0.005 < \Delta U/U_\infty < 0.15$ {Eq.(10)}. To emphasize this similarity, we rewrite these results in different form: Huner's sidewall result is

$$\frac{U_\infty}{U_H} - 1 = 3.6\frac{\nu}{U_H d}\left(\frac{2\ell}{d}\right)^{0.5}\frac{d^2}{H^2} \tag{30}$$

and our bottom wall result is

$$\frac{\Delta U}{U_\infty} = 0.6\left(\frac{\nu}{Ud}\right)^{0.8}\left(\frac{2\ell}{d}\right)^{0.55}\frac{d^2}{L^2} \quad . \tag{31}$$

In both cases, when the boundary effect is not too large, the relative change in velocity is observed to depend inversely on the square of the distance from the wall and to vary inversely with the Reynolds number. In contrast, most boundary solutions based on the Stokes Equations[17] indicate an inverse dependence on the first power of the distance from the wall and are independent of the Reynolds number. Of course, it is possible that the Reynolds number of our experiment is not low enough for solutions of the Stokes equations to be valid; also, it is possible that the cylindrical geometry and the difficulties associated with the Stokes paradox are the cause of the difference. It is conceivable that for cylinders of finite length but large length to diameter ratio, inertia will continue to play a role in boundary effects even at extremely low Reynolds number.

It is clear that inertia is important in the range of Reynolds number of this experiment. This conclusion follows not only from Eq.(10) but also from the calculations based on the theory of de Mestre and Russel (Fig.10), which indicate that large values of the added mass coefficient can occur and can influence the results. Because of the lack of a rigorous solution for the added mass of a decelerating cylinder, it is not possible to draw strong conclusions from the difference between our observations and our calculations based on the de Mestre and Russel theory. However, this difference suggests that results based solely on solutions of the steady flow Stokes equations may be inadequate when the geometry is primarily two dimensional and accelerations are involved.

It is interesting to contrast our results with those obtained for a sphere approaching a plane wall. The theory of Brenner[18], based entirely on the Stokes equations without added mass terms, is in excellent agreement with the observations of MacKay, Suzuki, and Mason[19] and of Sutterby[20]. The experiments of Sutterby extend up to a Reynolds number (based on diameter) of 0.09 . Since our values of R_d for the cylinder are as low as 0.015, it would appear that our Reynolds number range overlaps that of Sutterby. However, R_d may not be the appropriate Reynolds number for comparing cylinders to spheres. If R_ℓ (based on length) is chosen, the ranges do not overlap. More likely, both length and diameter should be used; if the geometric mean $(2\ell d)^{\frac{1}{2}}$ is used, then the smallest value of $(2\ell d)^{\frac{1}{2}}U_\infty/\nu$ for our experiment is 0.0753 and the ranges do overlap slightly. Regardless of whether such comparisons can be made, it is clear that for boundary

effects involving deceleration at low Reynolds number, the use of the Stokes equations without added mass terms has strong experimental support for spheres but not for cylinders.

C. The Near Field Region

It is interesting to compare the result given in Eq.(13) (i.e., $dL/dt \propto L^{1/2}$) with similar results from the theory of lubrication. When two parallel planes approach each other at low Reynolds number (the "squeeze film" problem), it is well known[21] that $dL/dt \propto L^3$. When a sphere approaches closely to a plane[22], $dL/dt \propto L$. When a cylinder (radius a) approaches a plane, the result is more complicated, but for $L << a$, Michell[23] has obtained a result that implies $dL/dt \propto L^{3/2}$. Our observations ($L > a$) are not in the squeeze film region, but the squeeze film results suggest that Eq. (13) is probably not valid at extremely small distances. However, it is likely that the time spent in the squeeze film region is small compared to the time for which Eq.(13) is valid.

V. CONCLUSIONS AND SUGGESTIONS FOR FURTHER WORK

We have observed the velocity of a slender horizontal cylinder as it falls at low Reynolds number toward a horizontal plane boundary. From our observations we draw two main conclusions: (1) When the effect of the boundary is small, the relative change in velocity of the cylinder is inversely proportional to the square of the distance from the boundary, and (2) when the effect of the boundary is large, the deceleration of the cylinder is constant and the velocity is proportional to the square

root of the distance from the boundary. The first conclusion was observed to hold for more than two decades of Reynolds number ($0.015 < R_d < 2.86$) and the second for slightly more than one decade ($0.015 < R_d < 0.20$) .

Calculations based on the slender body theory of de Mestre and Russel do not agree well with our experimental results. The difference between the calculations and the experiment may be due to the Reynolds number of the experiment not being low enough or to an inadequate treatment of added mass. However, it is possible that the difference is due to more fundamental difficulties that arise when a low Reynolds number flow that is primarily two dimensional is represented by a distribution of Stokeslets. These difficulties may be removed if Oseenlets[24] are used instead of Stokeslets. Experiments at lower Reynolds number and derivations using Oseenlets are needed to settle this question.

In the range of Reynolds number of our experiment, the effects of added mass cannot be ignored. We have attempted to calculate the added mass by assuming that the decelerating cylinder behaves in a manner analogous to an oscillating cylinder in the decelerating phase of its swing. This approach ignores the previous history of the motion. It would be interesting to see if such an analogy would be successful for a sphere, where rigorous solutions are available both for the oscillating sphere (due to Stokes[25]) and for the sphere moving in an arbitrary manner (due to Basset[26]). Furthermore, it would be useful to have a solution for a cylinder moving in an arbitrary manner similar to Basset's solution for a sphere.

REFERENCES

* Present Address: Department of Physics, Lehigh University, Bethlehem, PA 18015

1. G.J. Hancock, Proc. Roy. Soc. (London) A217, 96 (1953).

2. M.J. Lighthill, Mathematical Biofluiddynamics (SIAM, Philadelphia, 1975) p. 45 and 141.

3. C. Brennan and H. Winet, in Annual Review of Fluid Mechanics, edited by M. Van Dyke, J.V. Wehausen, and J.L. Lumley, (Annual Reviews Inc., Palo Alto, California, 1977), Vol. 9, p. 339.

4. J.R. Blake, Proc. Camb. Phil. Soc. 70, 303 (1971).

5. J.R. Blake and A.T. Chwang, J. Eng. Math. 8, 23 (1974).

6. N.J. de Mestre, J. Fluid Mech. 58, 641 (1973).

7. J. Happel and H. Brenner, Low Reynolds Number Hydrodynamics (Prentice Hall, Englewood Cliffs, New Jersey, 1965) p. 323.

8. N.J. de Mestre and W.B. Russel, J. Eng. Math. 9, 81 (1975).

9. D.F. Katz, J.R. Blake, and S.L. Paveri-Fontana, J. Fluid Mech. 72, 529 (1975).

10. C.M. White, Proc. Roy. Soc. (London) A186, 472 (1946).

11. B. Huner and R.G. Hussey, Phys. Fluids 20, 1211 (1977)

12. S. Kaplun, J. Math. Mech. 6, 595 (1957).

13. H. Lamb, Philos. Mag. 21, 112 (1911).

14. G.K. Batchelor, J. Fluid Mech. 44, 419 (1970).

15. R.E. Williams and R.G. Hussey, Phys. Fluids 15, 2083 (1972); a typographical error (omission of the factor 4) is corrected here.

16. R.G. Hussey and J.M. Reynolds, Phys. Fluids 8, 1213 (1965).

17. See, for example, ref. 7, chapter 7.

18. H. Brenner, Chem. Engr. Sci. 16, 242 (1961).

19. G.D.M. MacKay, M. Suzuki, and S.G. Mason, J. Colloid Sci. 18, 103 (1963).

20. J.L. Sutterby, Trans. Soc. Rheol. 17, 575 (1973).

21. D.F. Moore, Principles and Applications of Tribology (Pergamon, New York, 1975) p. 113.

22. G.E. Charles and S.G. Mason, J. Colloid Sci. 15, 236 (1960).

23. A.G.M. Michell, Lubrication (Blackie & Son, London, 1950) p. 301.

24. A.T. Chwang and T.Y. Wu, J. Fluid Mech. 75, 677 (1976).

25. G.G. Stokes, Trans. Cambridge Phil. Soc. 9, 8 (1851).

26. A.B. Basset, Quart. J. Math. 41, 369 (1910).

27. A.T. Chwang, J. Fluid Mech. 72, 17 (1975).

28. J.M. Burgers, K. Ned. Adad. Wet. Verhand. 16, no. 4, 113 (1938).

29. S. Broersma, J. Chem. Phys. 32, 1626 (1960).

30. S. Broersma, J. Chem. Phys. 32, 1632 (1960).

31. E.O. Tuck, J. Fluid Mech. 18, 619 (1964).

32. R.G. Cox, J. Fluid Mech. 44, 791 (1970).

33. J.P.K. Tillett, J. Fluid Mech. 44, 401 (1970).

34. H. Brenner, J. Fluid Mech. 12, 35 (1962).

TABLES

FIGURES

APPENDIX and

VITA

TABLE I. Dimensions and masses of the cylinders.

Cylinder	Length 2ℓ(cm)	Diameter d(cm)	Mass m(g)	$\frac{2\ell}{d}$	$\epsilon=\{\ln(4\ell/d)\}^{-1}$
61 A	4.196	0.0987	0.2569	42.5	0.2251
B	3.040	0.0983	0.1836	30.9	0.2424
C	2.445	0.0979	0.1471	25.0	0.2557
D	2.217	0.0984	0.1342	22.5	0.2626
E	1.966	0.0981	0.1159	20.0	0.2709
F	1.670	0.0978	0.1006	17.1	0.2832
G	1.128	0.0982	0.0651	11.5	0.3190
75 A	2.570	0.0527	0.0453	48.8	0.2183
B	1.786	0.0529	0.0309	33.8	0.2374
D	1.305	0.0523	0.0225	25.0	0.2557
E	1.257	0.0525	0.0212	23.9	0.2585
F	1.100	0.0524	0.0189	21.0	0.2676

TABLE II. Displacements for Cylinder 61A with $\Delta t = 0.05$ sec.

i	D_i (cm)		
	ν=0.5	ν=1	ν=4cm^2/sec
1	0.1674	0.0476	0.0423
2	0.6700	0.3197	0.0343
3	0.7013	0.4517	0.0478
4	0.7069	0.4806	0.0655
5	0.7099	0.4889	0.0814
6	0.7103	0.4894	0.0980
7	0.7098	0.4941	0.1120
8	0.7102	0.5003	0.1236
9	0.7096	0.4986	0.1359
10	0.7126	0.4984	0.1481
11	0.7104	0.4974	0.1572
12	0.7099	0.5000	0.1639
13	0.7111	0.4991	0.1700
14	0.7089	0.4995	0.1767
15	0.7076	0.5007	0.1809
16	0.7088	0.4991	0.1858
17	0.7110	0.4995	0.1894
18	0.7122	0.4986	0.1937
19	0.7100	0.4984	0.1948
20	0.7095	0.4960	0.1972
21	0.7090	0.4987	0.1990
22		0.4941	0.2008
23			0.2020
24			0.2038
25			0.2037
26			0.2031
27			0.2048
28			0.2042
29			0.2047
30			0.2077
31			0.2071
32			0.2058

TABLE III. The constant velocity U_∞ and Reynolds number $R_d = U_\infty d/\nu$ when the cylinder is far from the bottom wall.

cylinder	ν cm^2/sec	U_∞ cm/sec	R_d	ν cm^2/sec	U_∞ cm/sec	R_d	ν cm^2/sec	U_∞ cm/sec	R_d
61 A	0.4897	14.20	2.862	1.034	9.969	0.9516	3.959	4.101	0.1022
B	0.4873	14.07	2.838	1.029	9.837	0.9397			
C	0.4864	13.93	2.804	1.028	9.690	0.9228			
D	0.4854	13.97	2.832	1.027	9.683	0.9278			
E	0.4845	13.95	2.824	1.026	9.599	0.9178			
F	0.4843	13.84	2.795	1.024	9.495	0.9068	3.959	3.536	0.0874
G	0.4835	13.59	2.760	1.022	9.118	0.8761			
75 A				1.063	4.061	0.2013	3.959	1.357	0.0181
B				1.061	3.911	0.1951			
D				1.062	3.792	0.1867			
E				1.064	3.737	0.1844	3.973	1.164	0.0154
F				1.068	3.667	0.1799			

TABLE IV. Five cases of constant deceleration.

case	cylinder	ν cm^2/sec	R_d	Δt sec	d^2L/dt^2 cm/sec^2
I	75A	1.063	0.2013	0.05	12.47
II	61A	3.959	0.1022	0.05	6.34
III	61F	3.959	0.0874	0.05	5.46
IV	75A	3.959	0.0181	0.10	0.882
V	75E	3.973	0.0154	0.20	0.757

TABLE V. Near field displacements for the five cases of Table IV.

	D_i (cm)				
i	I	II	III	IV	V
1	0.0550	0.0423	0.0398	0.0337	0.0349
2	0.0758	0.0343	0.0386	0.0245	0.0588
3	0.1140	0.0478	0.0502	0.0343	0.0919
4	0.1381	0.0655	0.0655	0.0398	0.1194
5		0.0814	0.0802	0.0514	0.1504
6		0.0980	0.0931	0.0600	
7		0.1120	0.1071		

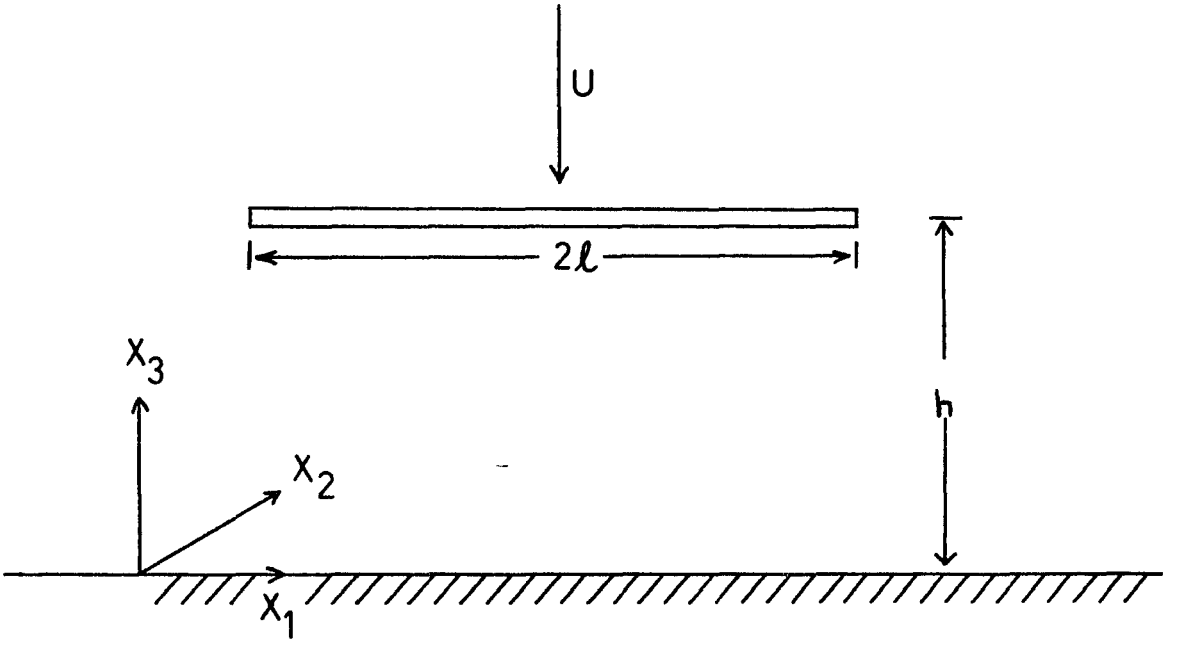

FIGURE 1A

A Schematic Diagram of a Cylindrical Rod of Diameter d and Length 2ℓ Moving with a Terminal Velocity U through a Viscous Fluid with its Axis a distance h away from the Wall

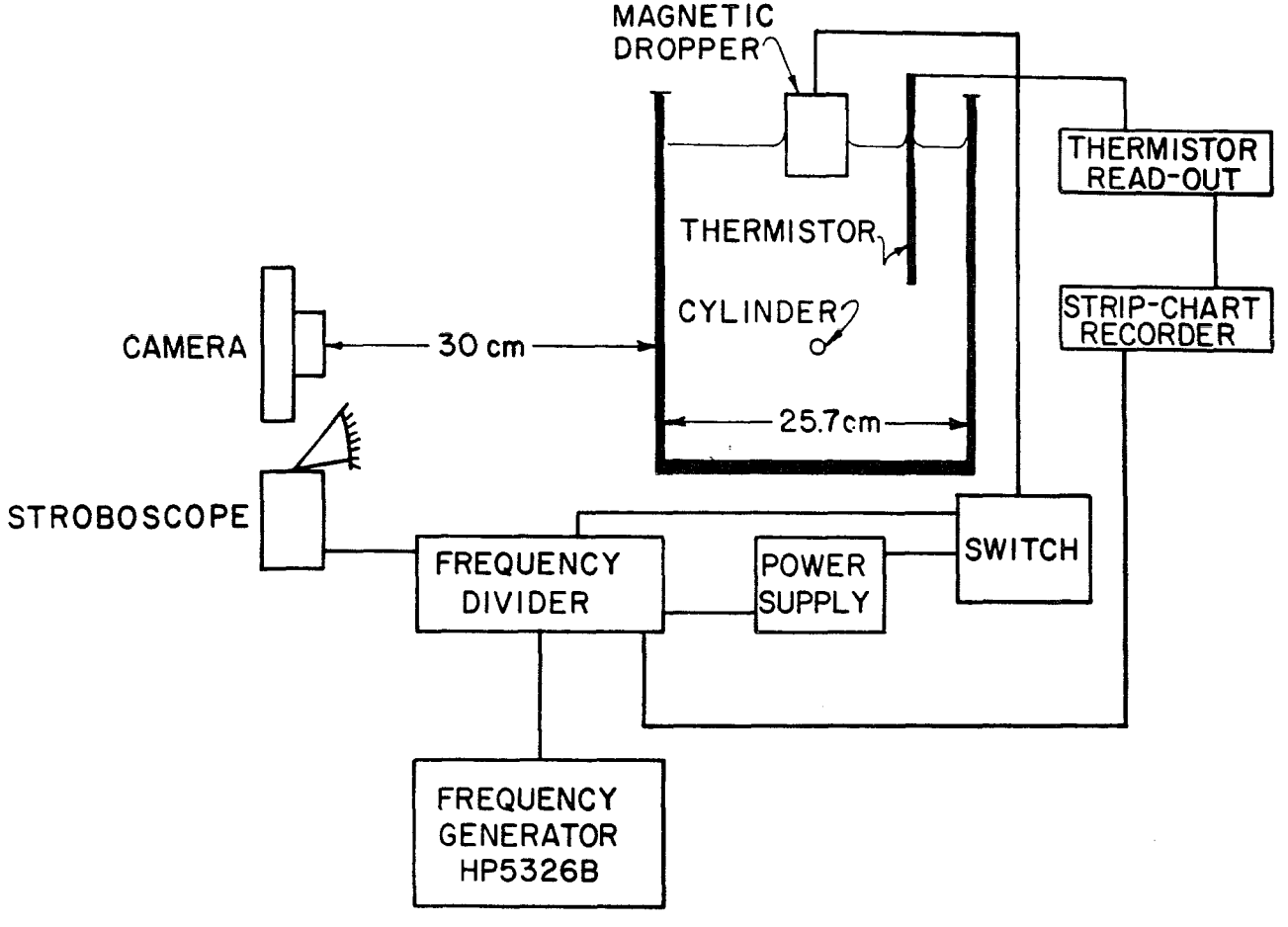

FIGURE 1

The Experimental Arrangement

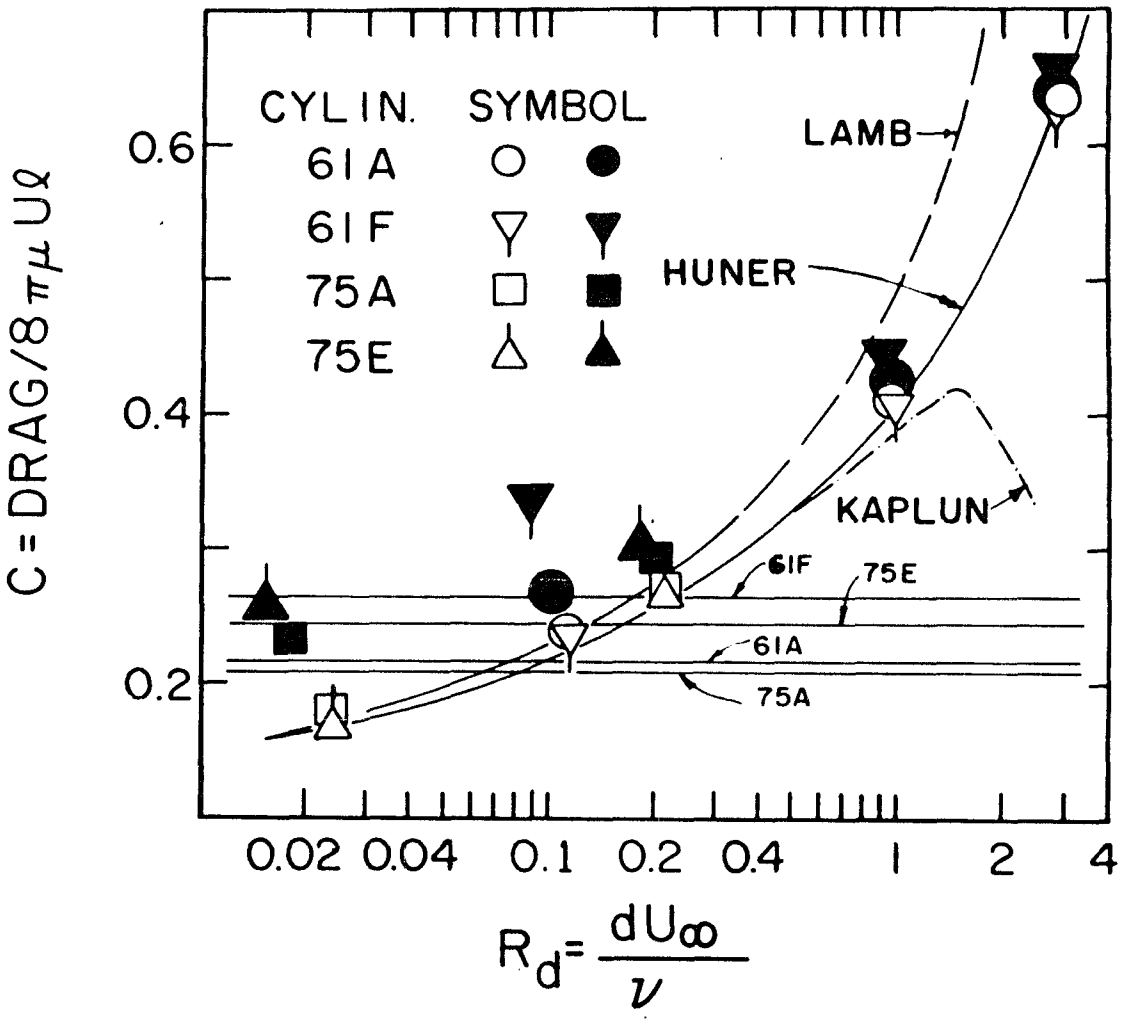

FIGURE 2

The Dimensionless Drag in the Region of Constant Velocity. The Closed Symbols are Data for Cylinders of Finite Length. The Open Symbols are the same Data Extrapolated to Infinite Length. The Horizontal Lines are the Values Obtained from Eq. (7)

FIGURE 3

An Empirical Correlation of Data in the Transition Region

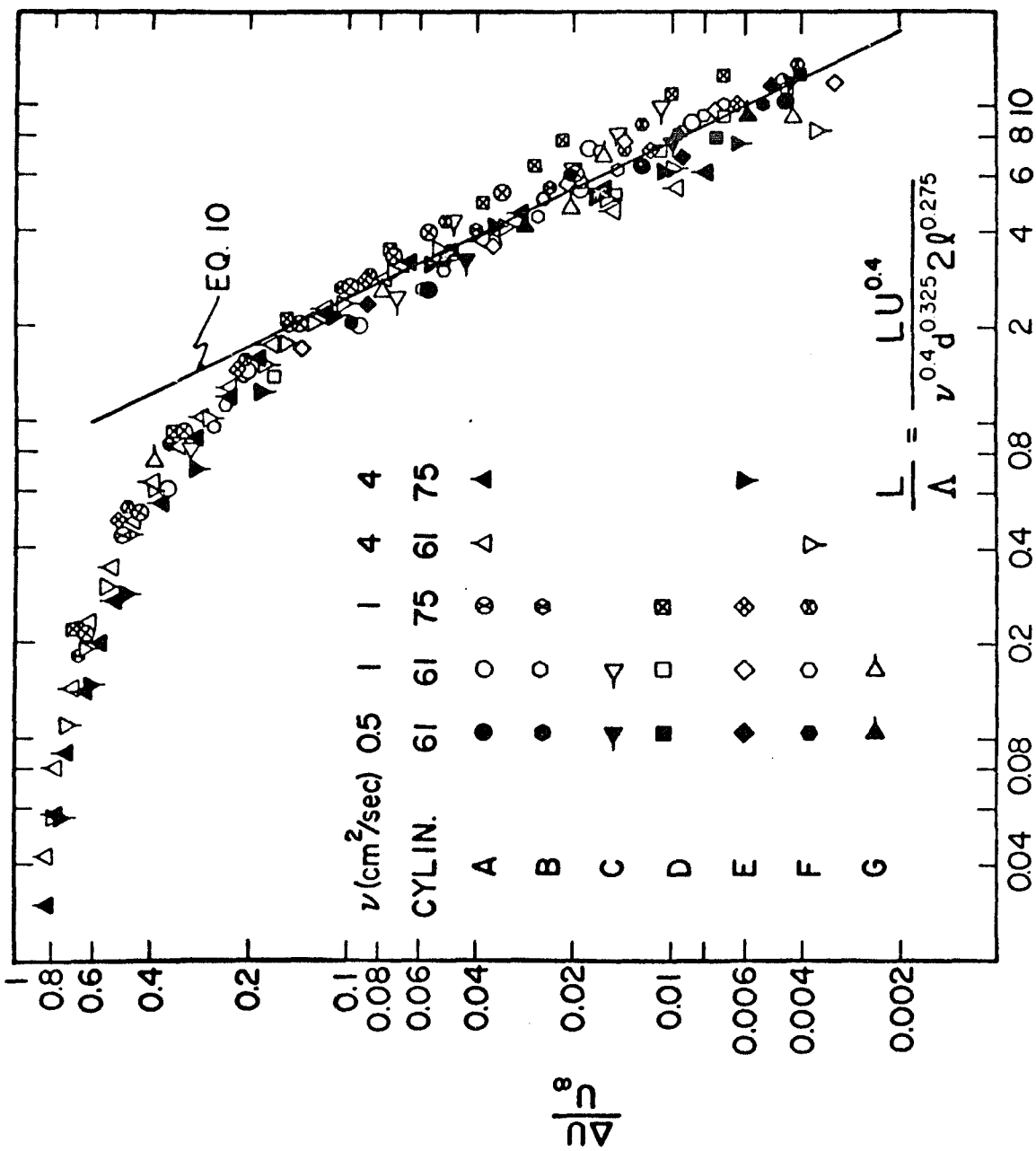

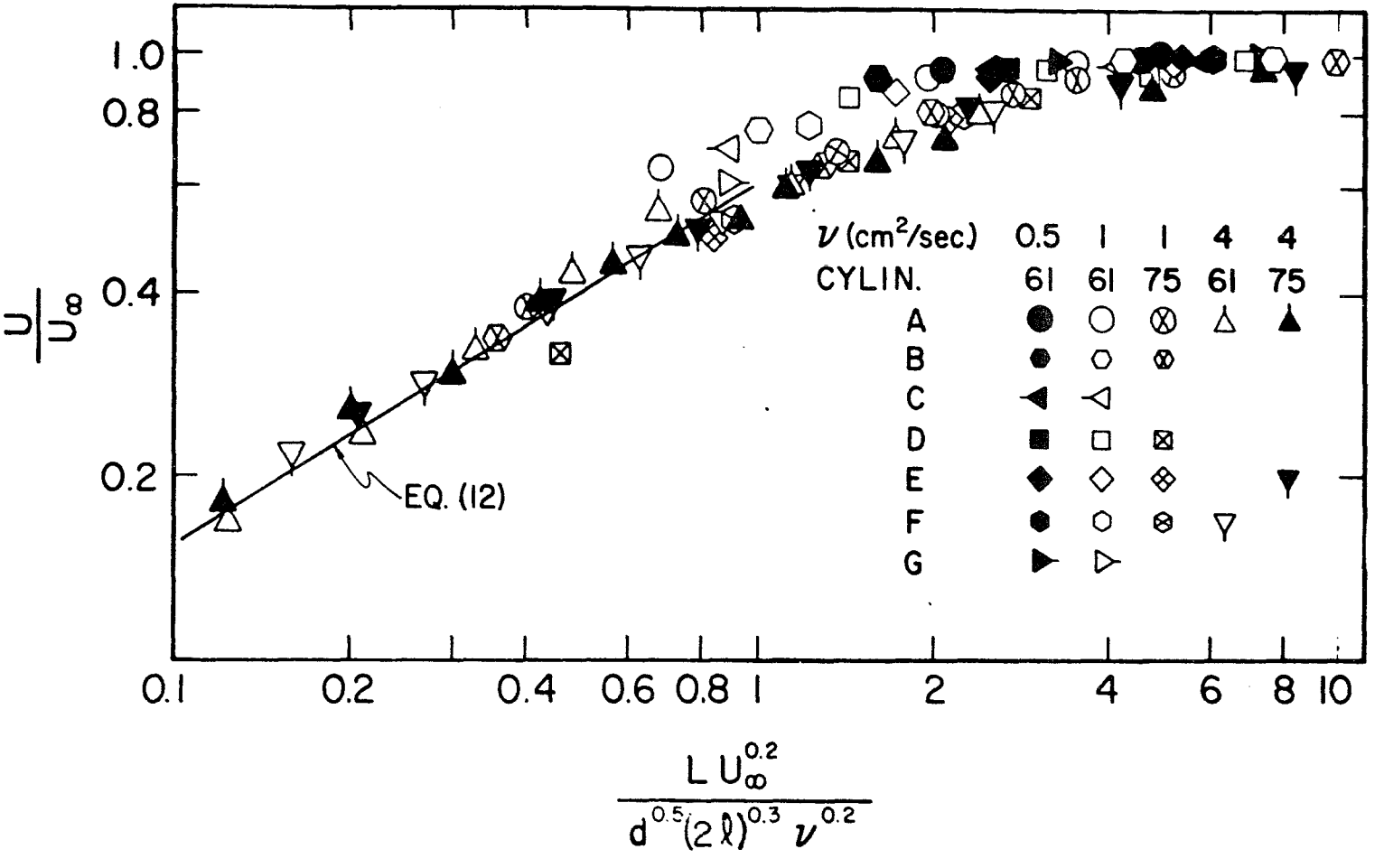

FIGURE 4

An Empirical Correlation of Data in the Near Field Region. The Symbols are the same as in Fig. 3

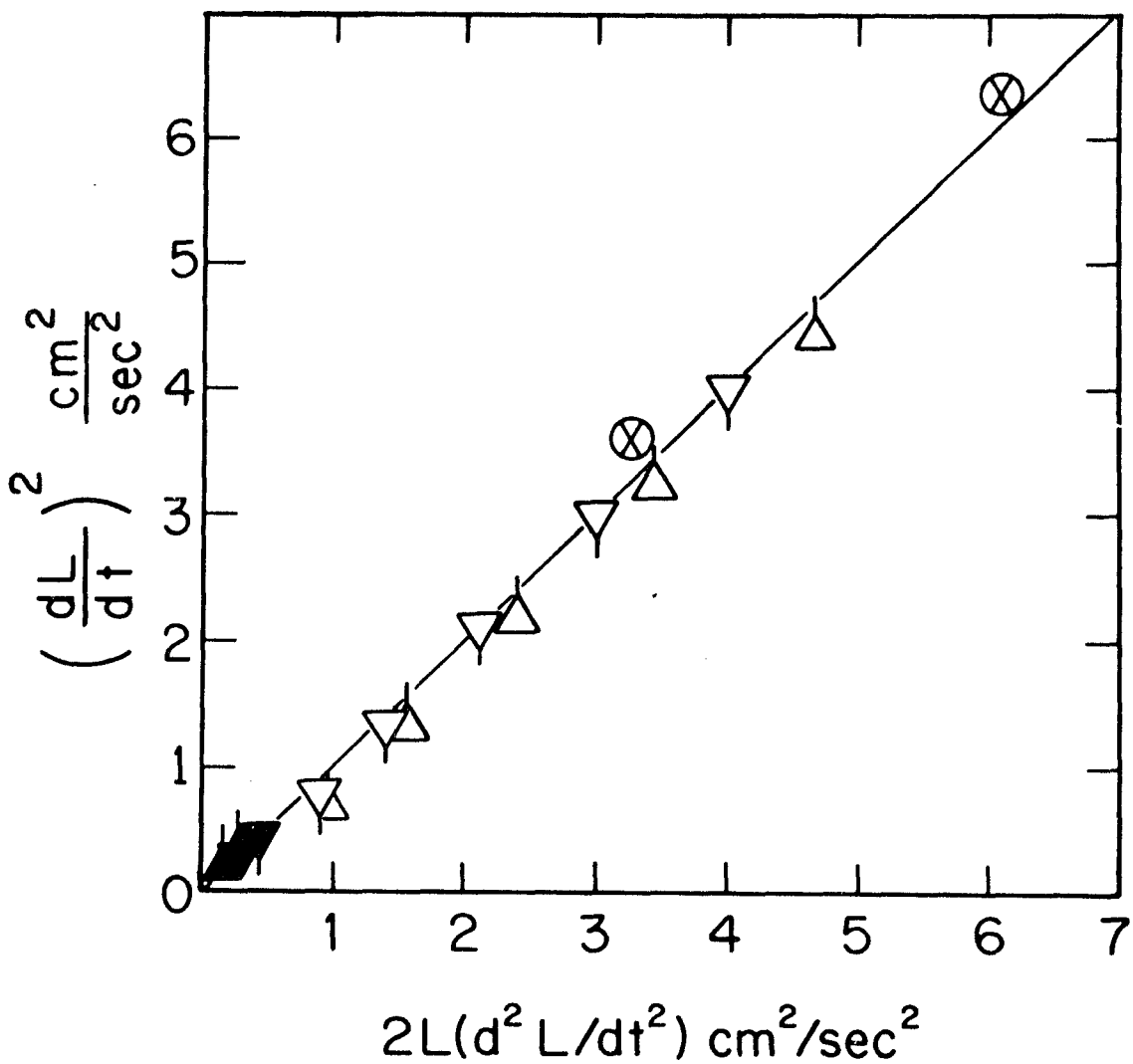

FIGURE 5

Data in the Region of Constant Deceleration. The Symbols are the same as in Fig. 6 . The Straight Line is Eq. (13)

FIGURE 6

The Dependence of the Dimensionless Deceleration on the Reynolds Number R_d and the Length to Diameter Ratio $2\ell/d$. The Straight Line is Eq. (14)

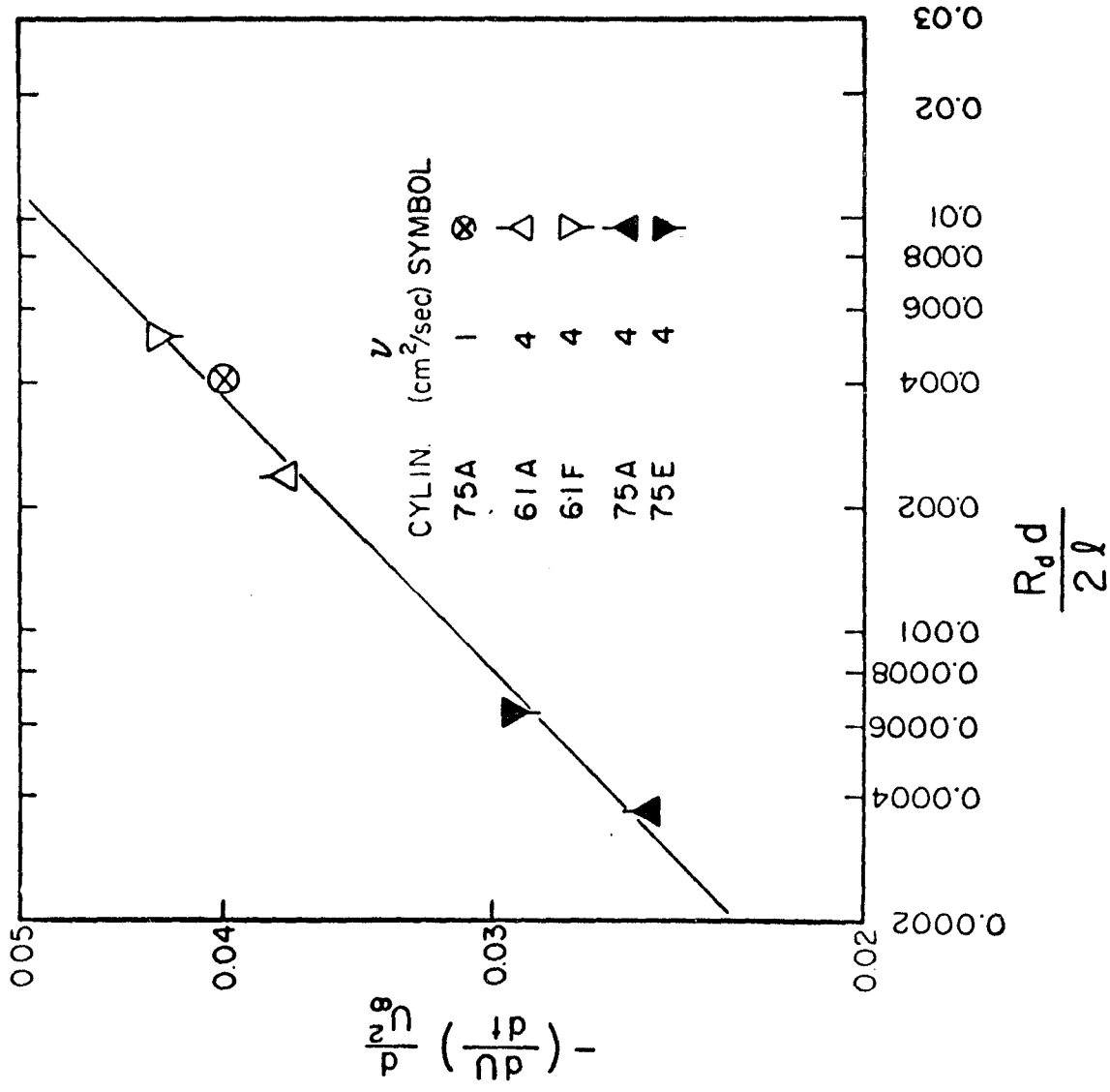

FIGURE 7

The Influence of the Sidewalls on the Terminal Velocity

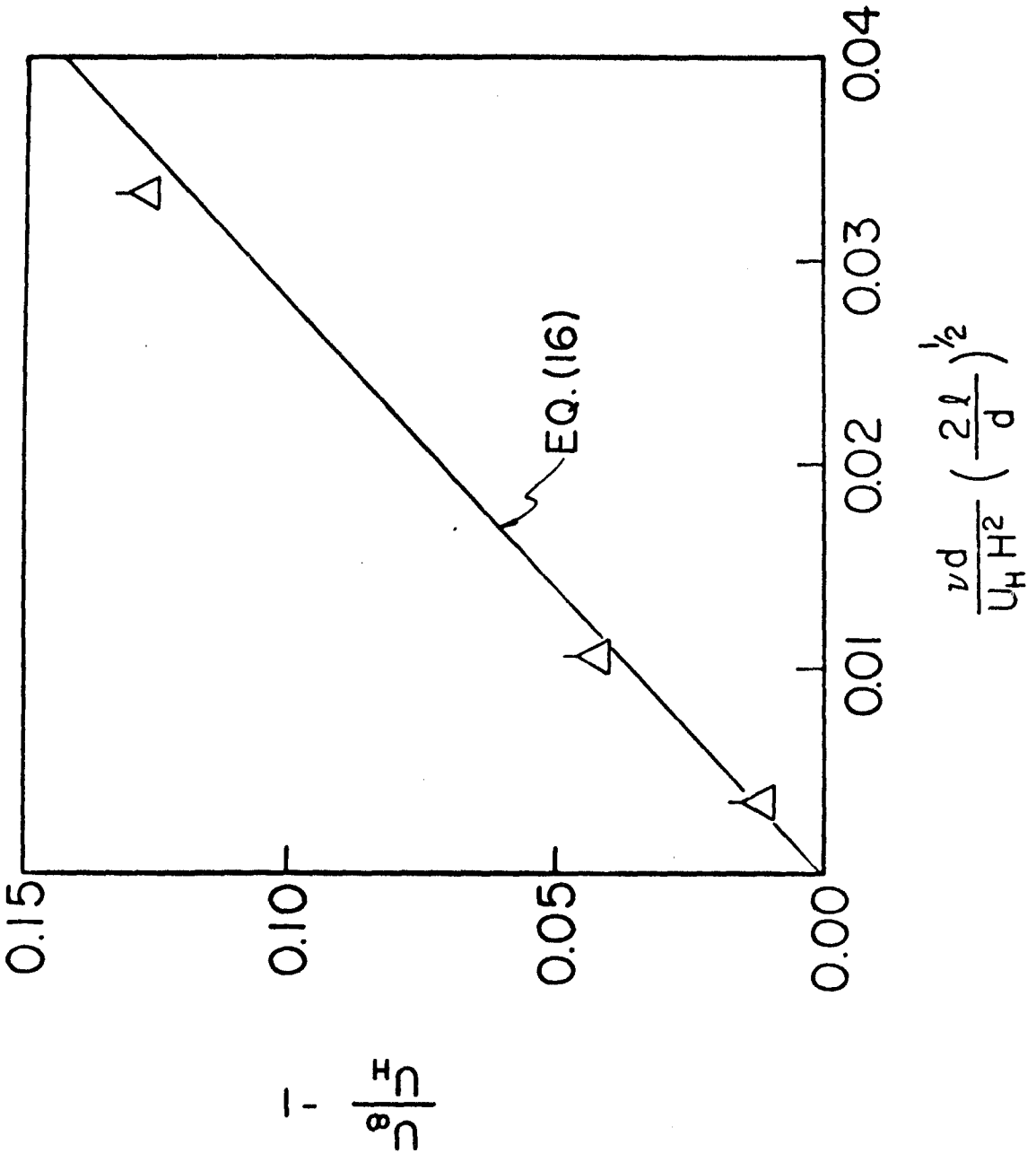

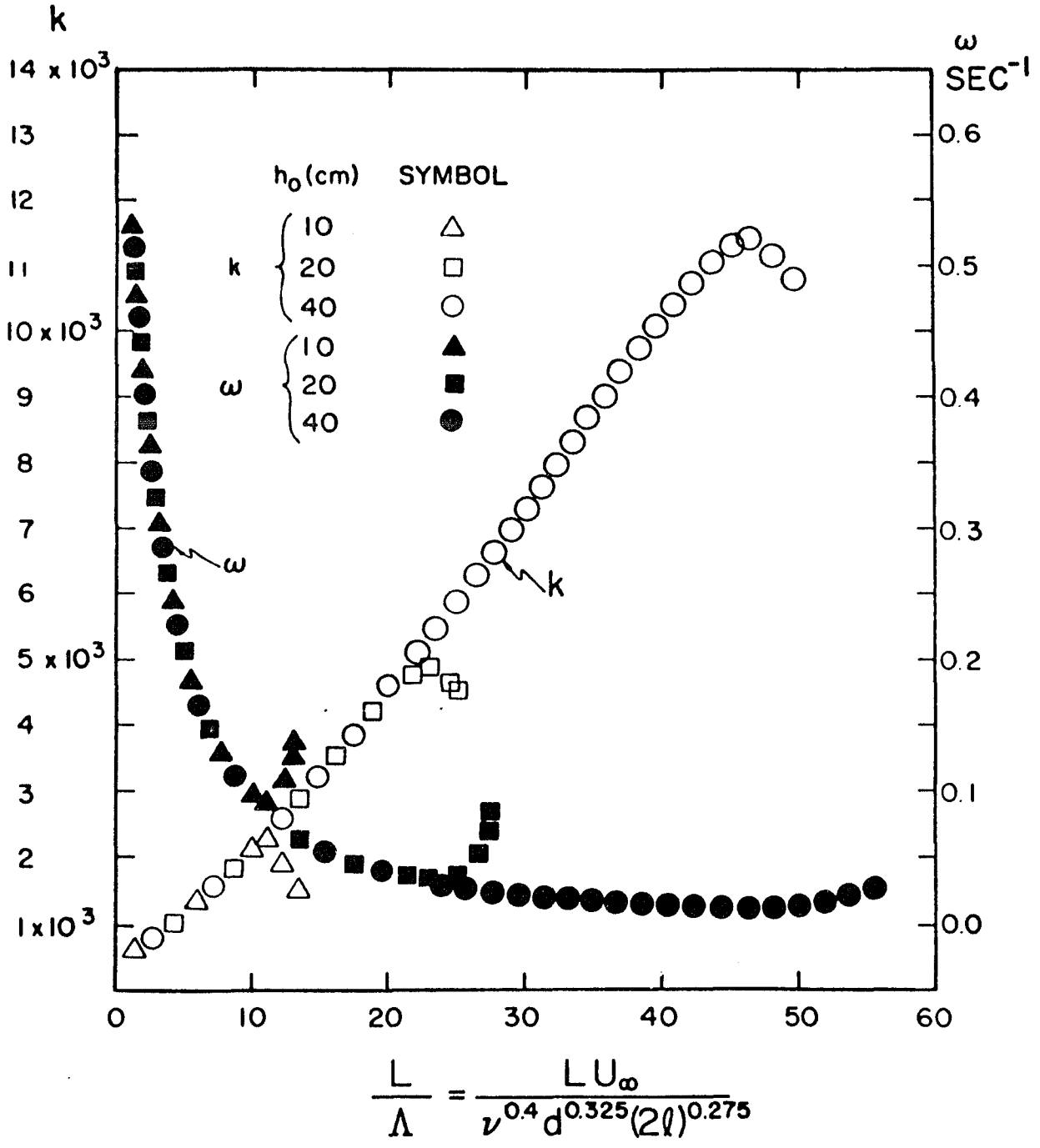

FIGURE 8

Dependence of the Calculated Added Mass Coefficient k and Circular Frequency ω on the Starting Position h_0 .

FIGURE 9

Comparison Between the Calculated Values (Numbered Curves) and the Experimental Curve in the Transition Region

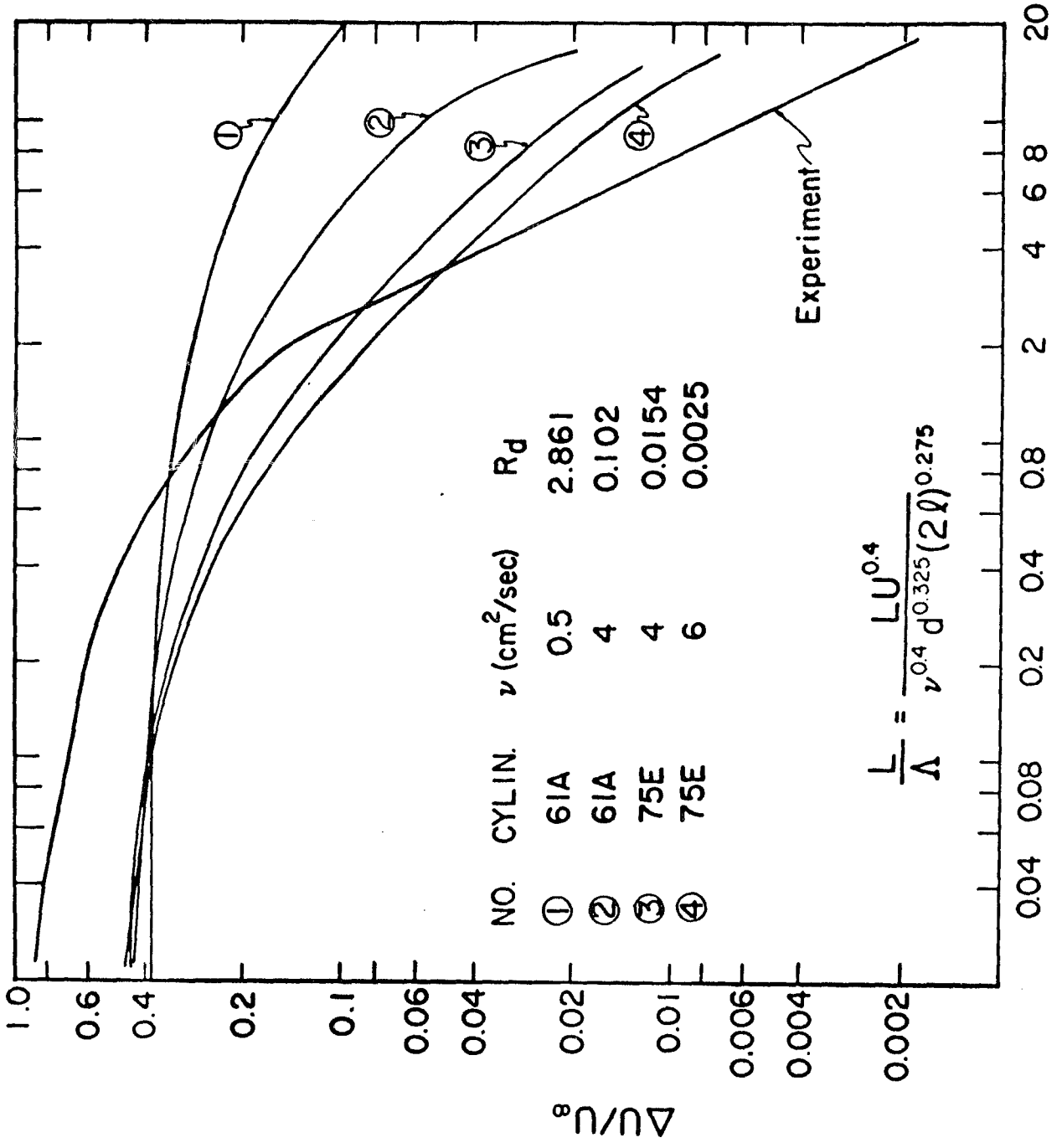

FIGURE 10

The Effect of Added Mass on the Calculated Values of $\Delta U/U_\infty$ in the Transition Region. The Calculations are for Cylinder 75 E in the 4 cm^2/sec Fluid

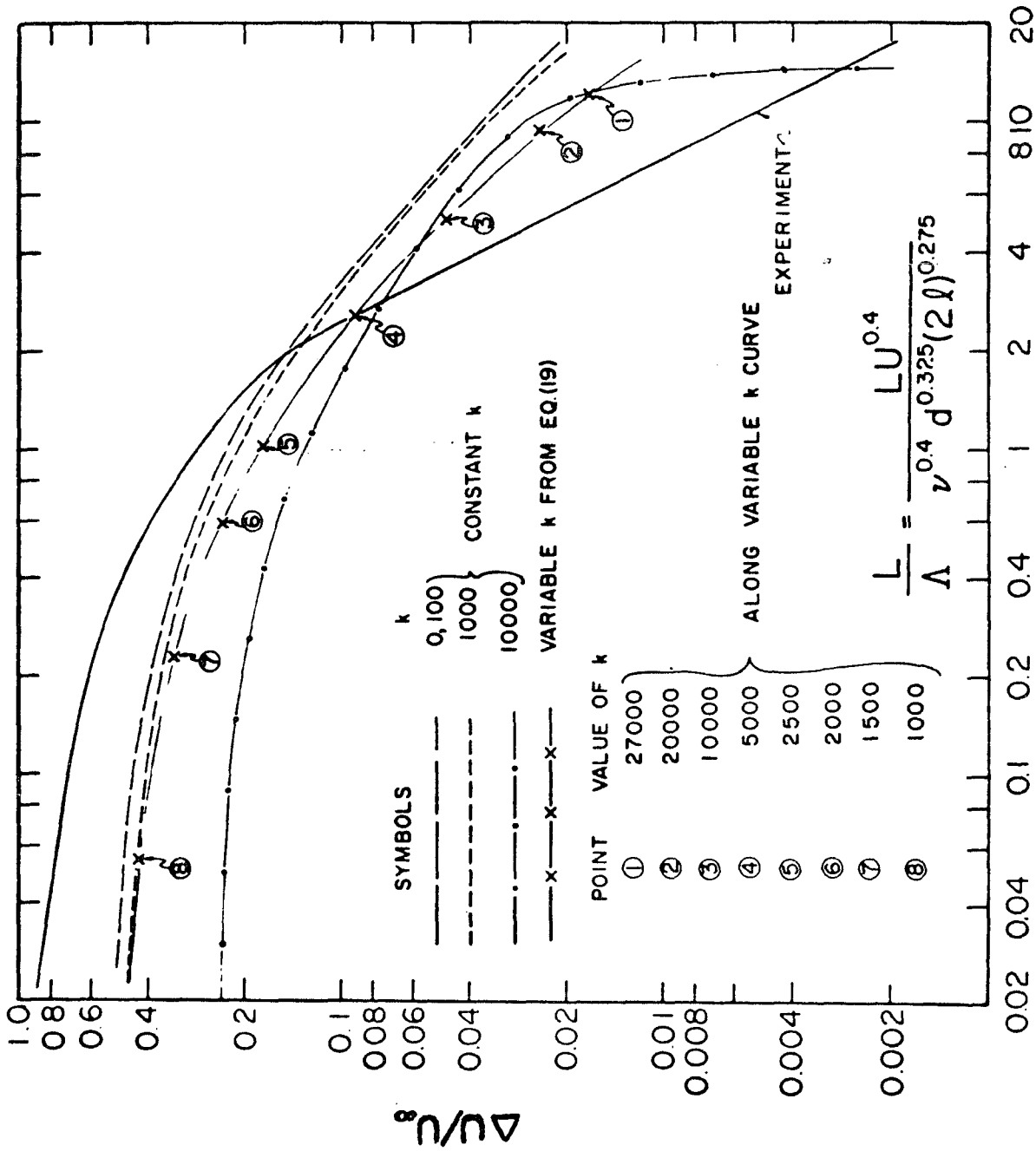

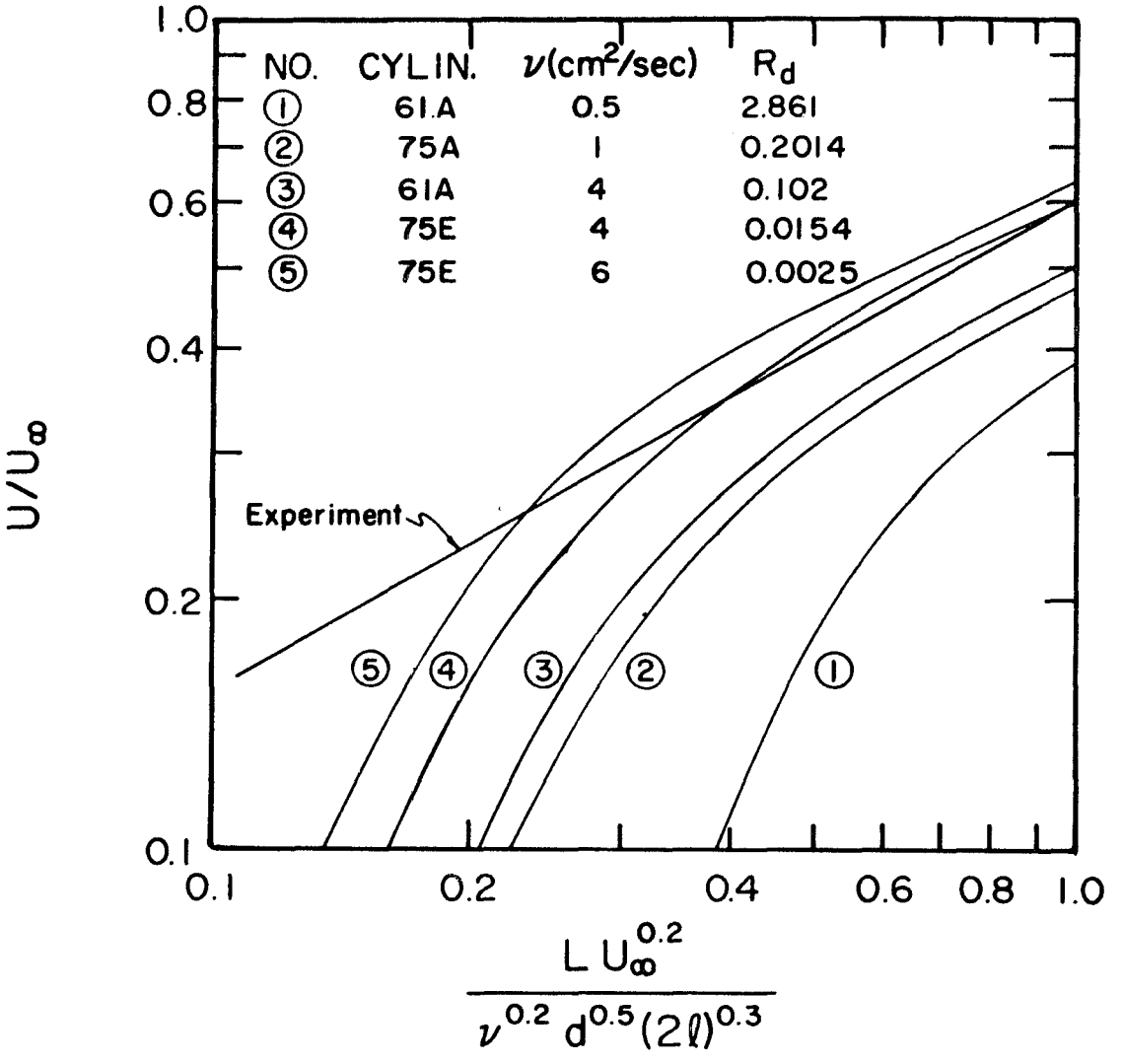

FIGURE 11

Comparison Between the Calculated Values (Numbered Curves) and the Experimental Curve in the Near Field

APPENDIX I

For the case of a circular cylinder (radius a) moving through inviscid fluid toward a parallel plane boundary as shown in Fig. A1 (a distance b from the cylinder axis), the successive image method[16] is applied here to derive an expression for the added mass coefficient k(a•b) . Consider the cylinder to be moving perpendicular to its axis toward the parallel plane wall in an imcompressible, inviscid fluid and suppose that the flow of the fluid is irrotational and is due entirely to the motion of the cylinder. Let the origin of coordinates coincide instantaneously with the center of the cylinder. Under these conditions, the total added mass per unit length M, contributed from a doublet at the origin and its images, can be written as

$$M = M_0 + M_{ij}$$

$$M_{ij} = -\rho \int \phi_{ij} \left(\frac{2\phi_{ij}}{2n}\right) dS$$

i = nth image, i = 1,2,3...n

j = 1 or 2, 1 means image in plane

2 means image in cylinder

where ρ is the density of the fluid, M_0 is the added mass per unit length contributed from the doublet at the origin and ϕ_{ij} is the velocity potential per unit velocity. The normal derivative of

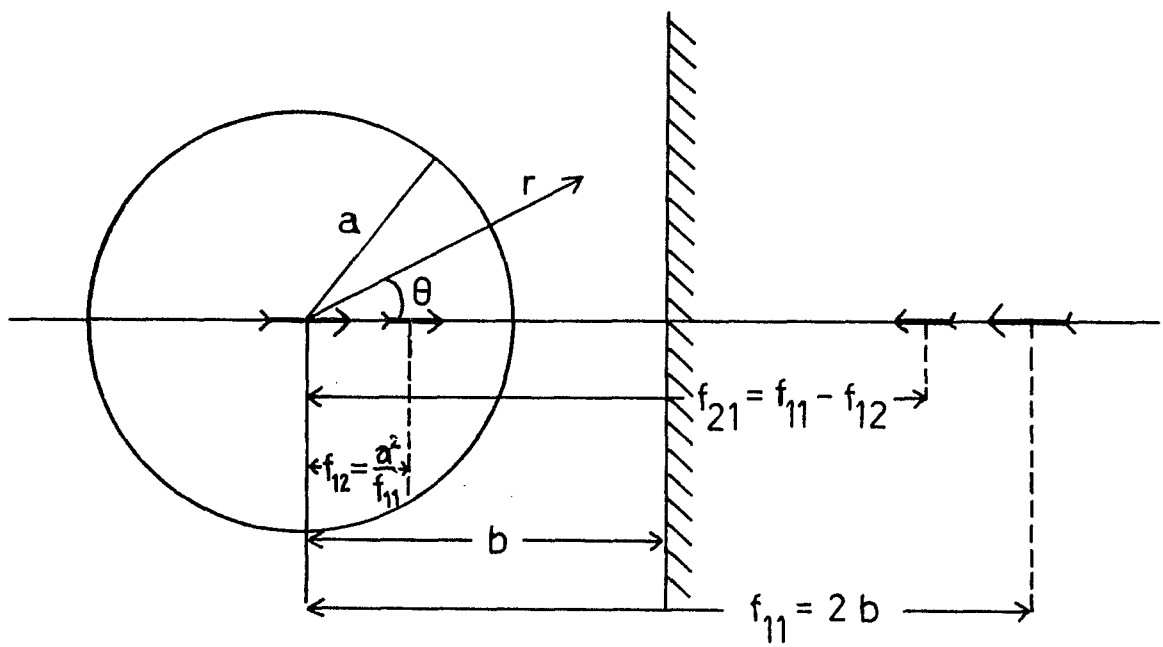

FIGURE A1

A Schematic Diagram for the Case of a Circular Cylinder (Radius a) Moving through Inviscid Fluid toward a Parallel Plane Boundary

velocity potential at the surface of the cylinder is determined by the boundary condition

$$\left(\frac{\partial \phi_{ij}}{\partial n}\right)_{r=a} = \left(\frac{\partial \phi_{ij}}{\partial r}\right)_{r=a} = -\cos\theta$$

since $\bar{n}$ and $\bar{r}$ have the same direction. The velocity potentials due to the doublet and its images are the real part of the complex potential W_{ij}, which can be obtained by the successive image method, i.e.

$$\phi_{ij} = \text{Real } (W_{ij})$$

The horizontal line passing through the center of the cylinder is considered as the real axis and the doublet and its images are all situated on and parallel to the real axis. The complex potentials of those images can be expressed in the form

$$W_{ij} = \frac{(-1)^j \mu_{i,j}}{Z - f_{i,j}} \qquad \begin{matrix} i = 1,2,3... \\ j = 1 \text{ or } 2 \end{matrix}$$

where $Z = re^{i\theta}$. The μ_{ij}'s are the strengths of the images and have the following relations.

$$\mu_{1,1} = \mu_0 = a^2$$

$$\mu_{i,1} = \mu_{i-1,2} \qquad i = 2,3,4$$

$$\mu_{i,2} = \mu_{i,1} \times \frac{a^2}{f_{i,1}} \qquad i = 1,2,3...$$

where a is the radius of the cylinder, the f_{ij}'s are the locations of the images and have the relations

$$f_{1,1} = 2b$$

$$f_{i+1,1} = f_{i,1} - f_{i,2} \qquad i = 1,2,3...$$

$$f_{i,1} \times f_{i,2} = a^2 \qquad i = 1,2,3...$$

and b is the distance from the center of the cylinder to the plane boundary.

The contribution of the images in the plane boundary to the added mass per unit length is obtained by

$$M_{i1} = \rho a^2 \int_0^{2\pi} \frac{(f_{i,1} - a\cos\theta)\cos\theta}{f_{i,1}+a^2-2af_{i,1}\cos\theta} d\theta$$

Integration under the condition $\frac{f_{i,j}}{a} > 1$, in the complex plane shows that this definite integral has the value

$$M_{i1} = \pi a^2 \rho \frac{\mu_{i1}}{f_{i,1}} \qquad i = 1,2,3...$$

The added mass per unit length from the contribution of the images in the cylinder is

$$M_{i2} = \frac{\rho a^5}{f_{i,1}^2} \int_0^{2\pi} \frac{(a\cos\theta - f_{i,2})}{f_{i.2}^2+a^2-2af_{i,2}\cos\theta} d\theta$$

Under the condition $\frac{a}{f_{i,2}} > 1$, this integral also has the value

$$M_{i2} = \pi a^2 \rho \frac{\mu_{i1}}{f_{i,1}} \qquad i = 1,2,3...$$

These results enable us to write the total added mass

$$M = M_0 + \sum_{i}^{n} \sum_{j=1.2} \mu_{ij}$$

$$= \pi a^2 \rho \{ 1 + \sum_{i}^{n} \frac{2\mu_{ij}}{f_{i,1}} \} \qquad i = 1,2,3...$$

If we define $\varepsilon = a/2b$, the first five terms of the above equation can be written as

$$M = \pi a^2 \rho \{ 1 + 2\varepsilon^2 + 2 \frac{\varepsilon^4}{(1-\varepsilon^2)^2} + 2 \frac{\varepsilon^6}{(1-2\varepsilon^2)^2} + \frac{2\varepsilon^8}{((1-\varepsilon^2)-\varepsilon^2)^2} \}$$

$$= \pi \rho a^2 K(a.b)$$

APPENDIX II

In this appendix, we derive a result from the theory of lubrication. The result was quoted without proof by Michell[23].

Consider a cylindrical rod of radius R and length ℓ moving towards the plane as shown in Fig. A2 . It displaces the liquid horizontally outwards with velocity U, which varies with both the radius r and with the distance Z from the plane, Z being less than Z_0, above which the pressure p is zero. Since Z_0 is assumed to be large compared with h at all times, the velocity U will be negligibly small both where the film thickness is Z_0 and on the cylinder where $Z = Z_1$. Thus the equation of motion can be written as

$$\mu \frac{\partial^2 U}{\partial Z^2} dZ = \frac{\partial p}{\partial r} \cdot dZ$$

$$\mu U = \frac{\partial p}{\partial r} \left(\tfrac{1}{2} Z^2 + CZ + D \right)$$

U=0, both when Z=0 and when $Z=Z_1$, D=0 and $C=-\tfrac{1}{2}Z_1$

so that $U = \frac{1}{2\mu} \frac{\partial p}{\partial r} (Z^2 - ZZ_1)$

and the total outward flow taken along the whole length at r, from Z=0 to $Z=Z_1$, will be

$$2\ell \int_0^{Z_1} U dZ = \frac{2\ell}{\mu} \cdot \frac{\partial p}{\partial r} \int_0^{Z_1} (Z^2 - ZZ_1) dZ$$

$$= - \frac{2\ell}{\mu} \frac{\partial p}{\partial r} \frac{Z_1^3}{6}$$

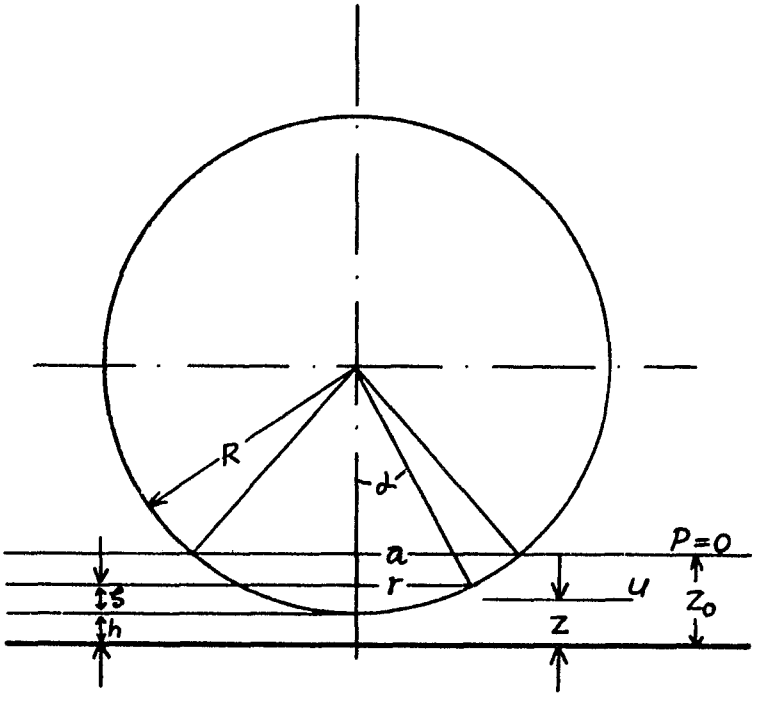

FIGURE A2

A Schematic Diagram for a Cylindrical Rod of Radius R and Length ℓ Moving toward the Plane

If for Z_1 can be written $h+\zeta$, where $\zeta = \frac{r^2}{2R}$, the total flow is

$$-\frac{2\ell}{6U}\frac{\partial p}{\partial r}\left(h + \frac{r^2}{2R}\right)^3 = \frac{-2}{6\mu}\frac{\partial p}{\partial r}\frac{1}{8R^3}\left(2Rh + r^3\right)^3$$

$$= -2r\ell\frac{\partial h}{\partial t}$$

The right-hand member of the equation is the volume of fluid displaced from beneath the cylinder, from the normal line through its center to the radius r.

Therefore

$$\frac{\partial p}{\partial r} = K\frac{\partial h}{\partial t}\frac{r}{\left(2Rh + r^2\right)^3}$$

where $K = 48\mu R^3$, and integrating

$$p = -K\frac{\partial h}{\partial t}\frac{1}{4\left(2Rh + r^2\right)^2} + L$$

But $p = 0$ at $r = a$

therefore,

$$L = K\frac{\partial h}{\partial t}\frac{1}{4\left(2Rh + a^2\right)^2}$$

and

$$p = -\frac{K}{4}\frac{\partial h}{\partial t}\left\{\frac{1}{\left(2Rh + r^2\right)^2} - \frac{1}{\left(2Rh + a^2\right)^2}\right\}$$

By a further integration is found the total fluid pressure to the radius $r = a$, by which the weight of the cylinder is supported:

$$p = \int_0^a 2\ell p dr$$

Beyond $r = a$, since the velocity is negligibly small, the pressure, being zero at $Z = 0$, is negligibly small through the film.

Thus

$$p = \frac{-K\ell}{2} \frac{\partial h}{\partial t} \int_0^a \{ \frac{1}{(2Rh + r^2)^2} - \frac{1}{(2Rh + a^2)^2} \} \, dr$$

from which is found

$$p = \frac{-K\ell}{2} \frac{\partial h}{\partial t} \{ \frac{a}{4Rh(a^2 + 2Rh)} + \frac{1}{2(2Rh)^{3/2}} \tan^{-1} \frac{a}{\sqrt{2Rh}} - \frac{1}{(2Rh + a^2)^2} \}$$

Thus

$$t = \int dt = \frac{-K\ell}{2p} \int_{h_0}^{h_1} \{ \frac{a}{4Rh\ (a^2 + 2Rh)} + \frac{1}{2(2Rh)^{3/2}} \tan^{-1} \frac{a}{\sqrt{2Rh}}$$

$$- \frac{a}{(2Rh + a^2)^2} \} \, dh$$

$$= t_1 + t_2 + t_3$$

$$t_1 = \frac{-K\ell}{8PRa} \ln \left(\frac{h_1(2Rh_0+a^2)}{h_0(2Rh_1+a^2)} \right)$$

$$t_2 = \frac{K\ell}{2(2R)^{3/2}p} \{ \frac{1}{\sqrt{h_1}} \tan^{-1}(\frac{a}{\sqrt{2Rh_1}}) - \frac{1}{\sqrt{h_0}} \tan^{-1} \frac{a}{\sqrt{2Rh_0}} \}$$

$$- \frac{K\ell}{8Rap} \{ \ln \frac{h_0\ (2Rh_1 + a^2)}{h_1\ (2Rh_0 + a^2)} \}$$

$$t_3 = \frac{K\ell a}{4PR} \left(\frac{h_0}{(2Rh_0 + a^2)} - \frac{h_1}{(2Rh_1 + a^2)} \right)$$

Substituting the value of K, we obtain

$$t = \frac{6\sqrt{2}\ \mu R^{3/2}\ell}{p}\left(\frac{1}{\sqrt{h_1}}\tan^{-1}\left(\frac{a}{\sqrt{2Rh_1}}\right) + \frac{1}{\sqrt{h_0}}\tan^{-1}\frac{a}{\sqrt{2Rh_0}}\right)$$

$$+ \frac{12R^2\ell a}{p}\left(\frac{h_0}{(2Rh_0 + a^2)} - \frac{h_1}{(2Rh_1 + a^2)}\right)$$

If a^2 is large in comparison with Rh_0 and Rh_1 ,

$$t = \frac{6\sqrt{2} \cdot \pi\mu R^{3/2}\ell}{p} \cdot \frac{h_1^{\frac{1}{2}} - h_0^{\frac{1}{2}}}{(h_1 h_0)^{\frac{1}{2}}}$$

APPENDIX III

a. TABLE VI. Displacements for Cylinder 61 Series in 0.5 cm^2/sec Fluid with $\Delta t = 0.05$ sec.

i	D_i (cm)					
	B	C	D	E	F	G
1	0.0388	0.1903	0.2123	0.0458	0.1462	0.2079
2	0.6349	0.6665	0.6647	0.6367	0.6568	0.6603
3	0.6891	0.6898	0.6933	0.6908	0.6854	0.6757
4	0.7000	0.6937	0.6955	0.6938	0.6920	0.6788
5	0.7030	0.6950	0.6976	0.6960	0.6924	0.6801
6	0.7034	0.6963	0.7015	0.6973	0.6928	0.6814
7	0.7055	0.6975	0.6993	0.6968	0.6941	0.6809
8	0.7042	0.6988	0.6988	0.6963	0.6910	0.6813
9	0.7037	0.6974	0.7000	0.6976	0.6905	0.6826
10	0.7040	0.6961	0.6987	0.6988	0.6900	0.6795
11	0.7035	0.6965	0.6990	0.6957	0.6921	0.6773
12	0.7048	0.6986	0.6968	0.6987	0.6908	0.6794
13	0.7034	0.6972	0.6963	0.6956	0.6921	0.6816
14	0.7029	0.6976	0.6985	0.6977	0.6933	0.6803
15	0.7033	0.6954	0.6988	0.6972	0.6946	0.6789
16	0.7035	0.6974	0.7001			0.6807
17	0.7021	0.6952				
18	0.7042					
19	0.7037					
20	0.7058					
21	0.7027					

b. TABLE VII. Displacements for Cylinder 61 Series in 1 cm^2/sec Fluid with $\Delta t = 0.05$ sec.

i	D_i (cm)					
	B	C	D	E	F	G
1	0.0973	0.0640	0.1577	0.2117	0.1023	0.0455
2	0.3659	0.3368	0.4028	0.4134	0.3602	0.2778
3	0.4630	0.4503	0.4552	0.4629	0.4502	0.4205
4	0.4791	0.4614	0.4770	0.4698	0.4628	0.4466
5	0.4846	0.4747	0.4789	0.4732	0.4669	0.4485
6	0.4872	0.4773	0.4808	0.4765	0.4709	0.4540
7	0.4884	0.4792	0.4820	0.4784	0.4742	0.4538
8	0.4896	0.4783	0.4853	0.4810	0.4719	0.4557
9	0.4908	0.4845	0.4844	0.4808	0.4717	0.4555
10	0.4941	0.4828	0.4856	0.4813	0.4743	0.4560
11	0.4953	0.4826	0.4832	0.4790	0.4762	0.4551
12	0.4929	0.4873	0.4858	0.4809	0.4760	0.4564
13	0.4920	0.4878	0.4835	0.4778	0.4744	0.4583
14	0.4925	0.4834	0.4833	0.4811	0.4735	0.4553
15	0.4922	0.4860	0.4845	0.4823	0.4747	0.4565
16	0.4911	0.4864	0.4828	0.4800	0.4752	0.4570
17	0.4908	0.4827	0.4840	0.4791	0.4764	0.4561
18	0.4892	0.4832	0.4859	0.4810	0.4726	0.4545
19	0.4890	0.4830	0.4843	0.4793	0.4724	0.4529
20	0.4896		0.4826	0.4784	0.4743	0.4548
21	0.4927			0.4790	0.4755	0.4560
22	0.4901				0.4763	0.4572
23	0.4918					0.4558
24	0.4907					0.4568
25	0.4931					

c. TABLE VIII. Displacements for Cylinder 75 Series in 1 cm^2/sec Fluid

	D_i (cm)				
	A	B	D	E	F
i \ Δt(sec)	0.05	0.05	0.1	0.1	0.1
1	0.0550	0.0422	0.0282	0.0677	0.0704
2	0.0758	0.0657	0.1194	0.1844	0.1931
3	0.1140	0.0979	0.2494	0.2923	0.2896
4	0.1381	0.1267	0.3211	0.3411	0.3351
5	0.1609	0.1549	0.3511	0.3531	0.3484
6	0.1743	0.1662	0.3644	0.3657	0.3597
7	0.1829	0.1749	0.3690	0.3689	0.3616
8	0.1883	0.1863	0.3709	0.3688	0.3621
9	0.1916	0.1876	0.3728	0.3714	0.3633
10	0.1929	0.1882	0.3753	0.3712	0.3652
11	0.1962	0.1909	0.3765	0.3725	0.3671
12	0.1989	0.1962	0.3784	0.3710	0.3663
13	0.1988	0.1921	0.3789	0.3749	0.3669
14	0.2035	0.1974	0.3795	0.3768	0.3654
15	0.2028	0.1974	0.3780	0.3740	0.3666
16	0.2014	0.1960	0.3806	0.3725	0.3672
17	0.2007	0.1933	0.3784	0.3730	0.3691
18	0.2027	0.1973	0.3810		0.3656
19	0.2033	0.1986	0.3775		
20	0.2039		0.3800		
21	0.2059				
22	0.2072				
23	0.2031				
24	0.2024				
25	0.2044				
26	0.2064				
27	0.2037				

d. TABLE IX. Displacements for Cylinder 61 and 75 Series in 4 cm^2/sec Fluid.

	D_i (cm)					
	61F	75A	75E		61F	75A	75E
i \ Δt(sec)	0.05	0.1	0.2	i			
1	0.0398	0.0337	0.0349	29	0.1762	0.1282	0.2343
2	0.0386	0.0245	0.0588	30	0.1762	0.1294	0.2336
3	0.0502	0.0343	0.0919	31	0.1792	0.1300	0.2342
4	0.0655	0.0398	0.1194	32	0.1791	0.1270	0.2335
5	0.0802	0.0514	0.1506	33	0.1754	0.1294	0.2328
6	0.0931	0.0600	0.1653	34	0.1785	0.1324	0.2322
7	0.1071	0.0667	0.1775	35	0.1766	0.1318	
8	0.1187	0.0729	0.1897	36	0.1778	0.1318	
9	0.1279	0.0802	0.2000	37		0.1330	
10	0.1377	0.0857	0.2067	38		0.1329	
11	0.1444	0.0887	0.2067	39		0.1347	
12	0.1493	0.0912	0.2115	40		0.1353	
13	0.1541	0.0961	0.2163	41		0.1335	
14	0.1584	0.1010	0.2199	42		0.1329	
15	0.1614	0.1046	0.2211	43		0.1341	
16	0.1638	0.1077	0.2223	44		0.1340	
17	0.1656	0.1089	0.2247	45		0.1346	
18	0.1674	0.1107	0.2264	46		0.1352	
19	0.1698	0.1113	0.2276	47		0.1364	
20	0.1710	0.1131	0.2288	48		0.1352	
21	0.1734	0.1174	0.2293	49		0.1364	
22	0.1746	0.1198	0.2286	50		0.1339	
23	0.1740	0.1210	0.2304	51		0.1375	
24	0.1752	0.1222	0.2322	52		0.1357	
25	0.1757	0.1240	0.2315	53		0.1369	
26	0.1763	0.1252	0.2327	54		0.1350	
27	0.1751	0.1258	0.2314	55		0.1362	
28	0.1756	0.1270	0.2325	56		0.1350	

APPENDIX IV

```
C       THIS PROGRAM IS TO USE THE FINITE METHOD TO SIMULATE THE MOTION
C       OF THE CYLINDER FALLING HORIZONTALLY APPROCH TO A PLANE BOUNDARY
C       FROM THE KNOWN DRAG
C       THE FAR FIELD DRAG IS FROM DEMWSTE AND RUSSEL THEORY
C       THE NEAR FIELD DRAG IS FROM KATZ BLAKE AND PAVERI-FONTANA
        DIMENSION U(7000), H(7000),AK(200)
100     FORMAT(2X,5(F11.6),F15.4,4(F14.6))
200     FORMAT(2(F6.3),F6.4,F6.3,5(F8.5),F8.3)
300     FORMAT(2X,9(F10.6),F12.3)
        READ(5,200)UINF,ZLC,DELTAT, DESTC,TTL,DESTF,VALUM,DIAM,VIS,FINF
        WRITE(6,300)UINF,ZLC,DELTAT,DESTC,TTL,DESTF,VALUM,DIAM,VIS,FINF
        RADIUS=DIAM/2
C       THE STARTING POINT FOR THE THE FAR FIELD IS
        U(1)=UINF
        H(I)=10
C       THE STARTING POINT FOR THE NEAR FIELD IS PICKED UP FROM EXP. DATA
C       THE FOLLOWING PROGRAM REPEATS THE PROCEDURE TO CALCULATE THE
C       VELOCITY WITH RESPECT TO IT'S RELATIVE POSITION.
7       DO 8 I=1,7000
        IF (I.EQ.1) GO TO 1
        H(I)=H(I-1)-U(I-1)*DELTAT
        IF(H(I)-RADIUS)6,1,1
1       RHTL=2*H(I)/ZLC
C       TO CACULATE THE ADDED MASS COEFF. IN INVICIDE FLUID CASE
        EP=DIAM/(4*H(I))
        EP1=EP**2
        EP2=2*EP**2
        EP3=2*EP**4/(1-EP**2)**2
        EP4=2*EP**6/(1-2*EP1)**2
        EP5=2*EP1**4/(1-3*EP1+EP1**2)**2
        BK=0+EP2+EP3+EP4+EP5
C       TO CACULATE THE DRAG DIFFERENCE FOR RELATIVE POINT INCLUDE WALL
C       EFFECT
        VISLTH=VIS/UINF
        RHT4=2*H(I)/(ZLC**0.75*DIAM**0.23*VISLTH**0.02)
        RRH=1/RHTL
        SIHP=ALOG(RRH+(RRH**2+1)**0.5)
        W=2*SIHP+(1/(1+RHTL**2)**0.5)
        EP6=(ALOG(1./EP))-1
C       THE NEAR FIELD DRAG DIFFERENCE IS
C       EP=(2*U(I)/(UINF*TTL*EP6*(2-0.386*TTL)))-1
C       THE FAR  FIELD DRAG DIFFERENCE IS
9       EP=(U(I)*1/UINF)*((2+TTL*(W-0.386))/(2-0.386*TTL))-1
```

```
      IF(I. GT . 1 ) GO TO 3
2     AK(1)=1
      GO TO 40
C     TO CACULATE THE ADDED MASS COEFF. IN VISCOUS FLUID CASE
3     AK(1)=AKI U
40    IF( I.GT. 0 ) GO TO 30
      DO 12 J=1,200
      XMASS=(DESTC+(AK(J)+BK)*DESTF)*VALUM
      UD=FINE*FD*DELTAT/XMASS
      WK=SQRT(2.*UD/UINF)/DELTAT
      CMASS=0.25*DIAM*(WK/VIS)**0.5
      X=2*CMASS
      A=0-ALOG(X/2.)-0.577222
      BSQ=A**2+(3.14159)**2/16
      B=BSQ**0.5
      Z0=B-(3.14159*(X/2)**2)/(4*B)+(A**2+(5*A)/2+2+((3.14159)**2*(1-2/B
     2SQ)/16))*(X/2)**4/(4*B)
      FA0=(1+A/BSQ)*(X/2)**2+(3.14159*(5/8+A/BSQ)*(X/2)**4)/(4*BSQ)-ATAN
     2(3.14159/(4*A))
      Z1=(1/X)-(3.14159*X/8+(A**2+3*A/2+7/8))*(X/2)**3
      FA1=1.25*3.14159-2*(A+0.5)*(X/2)**2-3.14159*(A+0.75)*(X/2)**4
500   FORMAT(2X,3(F20.7))
      AK(J+1)=1-(4*Z1)*COS(FA1-FA0-(0.75*3.14159))/(Z0*X)
      CAK=(AK(J+1)-AK(J))*100/AK(J+1)
      IF(CAK.GT.1) GO TO 12
20    AKI=AK(J+1)
      GO TO 5
12    CONTINUE
30    DO 15 J=1,200
      XMASS=(DESTC+(AK(J)+BK)*DESTF)*VALUM
      UD=FINF*FD*DELTAT/XMASS
      CSWT=U(I)/UINF
      TNWT=(1.-CSWT**2)**0.5/CSWT
      WK=((TNWT**2+2*UD/U(I))**0.5-TNWT)/DELTAT
      CMASS=0.25*DIAM*(WK/VIS)**0.5
      X=2*CMASS
      A=0-ALOG(X/2.)-0.577222
      BSQ=A**2+(3.14159)**2/16
      B=BSQ**0.5
      Z0=B-(3.14159*(X/2)**2)/(4*B)+(A**2+(5*A)/2+2+((3.14159)**2*(1-2/B
     2SQ)/16))*(X/2)**4/(4*B)
      FA0=(1+A/BSQ)*(X/2)**2+(3.14159*(5/8+A/BSQ)*(X/2)**4)/(4*BSQ)-ATAN
     2(3.14159/(4*A))
```

```
      Z1=(1/X)-(3.14159*X/8+(A**2+3*A/2+7/8))*(X/2)**3
      FA1=1.25*3.14159-2*(A+0.5)*(X/2)**2-3.14159*(A+0.75)*(X/2)**4
      AK(J+1)=1-(4*Z1)*COS(FA1-FA0-(0.75*3.14159))/(Z0*X)
      CAK=(AK(J+1)-AK(J))*100/AK(J+1)
400   FORMAT(2X,F12.5,11(F10.7))
      IF(CAK.GT.1) GO TO 15
      AKI=AK(J+1)
      GO TO 5
15    CONTINUE
5     U(I+1)=U(I)-UD
      CU=U(I)*100/UINF
      DU=(UINF-U(I))*100/UINF
      UL=(H(I)-RADIUS)*UINF**0.200/(VIS**0.200*DIAM**0.500*ZLC**0.300)
      VL=(H(I)-RADIUS)*U(I)**0.400/(VIS**0.400*DIAM**0.325*ZLC**0.275)
10    WRITE(6,100)H(I),     U(I),UD,WK,FD    ,AKI   ,UL,CU,DU,VL
8     CONTINUE
6     STOP
      END
C     THE SAMPLE DATA CARD FOR CYLINDER 61A  IN 50 C.S.
14.201 4.1960.0010 8.010 0.22506 0.95844 0.03208 0.09867 0.48970 221.554
```

VITA

Yang-jen Chen was born June 16, 1947 in Hsueh Chia, Tainan, Taiwan. He was educated in Hsueh Chia Elementary School and graduated from Tainan First High School in 1965. He attended Chung Yuan Christian College of Science and Engineering from which he received his Bachelor of Science Degree in 1969. He was commissioned as a second Lieutenant in the Chinese Air Force and completed his military service in July of 1970. He was an instructor in Department of Physics of his mother college for one year. He attended the Graduate School of the Louisiana State University in Baton Rouge, Louisiana in 1971. He is currently a candidate for the degree of Doctor of Philosophy in the Department of Physics, Louisiana State University.

EXAMINATION AND THESIS REPORT

Candidate: Yang-Jen Chen

Major Field: Physics

Title of Thesis: The Effect of a Horizontal Plane Boundary on a Falling Horizontal Cylinder at Low Reynolds Number

Approved:

Robert J. Hussey
Major Professor and Chairman

James D. Ingraham
Dean of the Graduate School

EXAMINING COMMITTEE:

A. Ravi Prakash Rao

Raymond F. Greenchik

Paul S. Lee

John T. Marshall

Date of Examination:

September 23, 1977